Supplementary Information

Nine undescribed sesquiterpenoids from the aerial parts of *Daphne penicillata*: cyclooxygenase-2 inhibition, molecular docking and molecular dynamics studies

Peng Zhao,[a] Ben-Song Xin,[a] Feng-Ming He,[b] Li Ye,[a] Zhen-Tao Ma,[a] Jin-Le Hao,[c] Rui Shi,[d] Xia-Hong He,[d] Guo-Dong Yao,[a] Bin Lin,[c] Xiao-Xiao Huang,[a] Shao-Jiang Song,[a,*]

[a] *Key Laboratory of Computational Chemistry-Based Natural Antitumor Drug Research & Development, Liaoning Province; Engineering Research Center of Natural Medicine Active Molecule Research & Development, Liaoning Province; Key Laboratory of Natural Bioactive Compounds Discovery & Modification, Shenyang; School of Traditional Chinese Materia Medica, Shenyang Pharmaceutical University, Shenyang, Liaoning 110016, China*

[b] *School of Pharmaceutical Sciences, Xiamen University, Xiamen, 361102, China*

[c] *Wuya College of Innovation, Shenyang Pharmaceutical University, Shenyang 110016, China*

[d] *Key Laboratory for Forest Resources Conservation and Utilization in the Southwest Mountains of China, Ministry of Education, International Ecological Foresty Research Center of Kunming, Horticulture and Landscape Architecture, Southwest Forestry University, Yunnan Kunming, 650224, China*

*Corresponding authors.

E-mail: songsj99@163.com (S. J. Song)

Table of Contents

1. Supplementary 1

1.1 Plant material.

The herbs of *Daphne penicillata* were collected from Wenchuan County, Aba Prefecture, Sichuan Province, China, in July 2019 (N31°29′51.52″, E103°38′14.35″). and authenticated by Prof. Jincai Lu (School of Traditional Chinese Materia Medica, Shenyang Pharmaceutical University). The voucher sample (No. MJ20190701) was deposited in the herbarium of Shenyang Pharmaceutical University.

1.2 Extraction and isolation

The dried herbs of *Daphne penicillata* (48.0 kg) were extracted under reflux conditions using 75% aqueous EtOH (50 L × 3 times × 4 hours). The percolates were combined and evaporated under reduced pressure to afford a crude extract. The extract was suspended in water and successively partitioned with EtOAc and *n*-BuOH. The EtOAc extract (600 g) and *n*-BuOH (1200 g) were subjected to silica gel column using CH_2Cl_2-MeOH (100:1-1:1, *v/v*) as gradient eluents to afford four fractions (Fr.A-D). Fr.C (150 g) was separated by polyamide chromatography eluted with 30% and 80% EtOH to obtain two fractions (Fr.C1 to Fr.C2), then Fr.C1 (75 g) was subjected to column chromatography on HP20 resin with H_2O, 30%, 60% and 90% EtOH to give two fractions (Fr.C1-1 and Fr.C1-3). Fr.C2-1 (28 g) were separated by ODS column chromatography, eluted with a gradient of MeOH-H_2O from 20:80 to 60:40, respectively. and then redistributed in five fractions (Fr.1-6) based on HPLC analysis. Among them, Fr.1 (15 g) was subjected to silica gel CC eluting with petroleum ether/EtOAc (*v/v*, 100:1 to 5:1) to yield five fractions (Fr.1.1–Fr.1.8). Fr.1.5 (2.4 g) and Fr.1.6 (3.5 g) were separated by preparative HPLC using MeOH/H_2O (48:52) to obtain the following fractions (Fr.1.2.1–Fr.1.5.8 and Fr.1.6.1–Fr.1.6.6). Fr.1.2.2 (98.2 mg) and Fr.1.2.3 (65.6 mg) were separated by semipreparative HPLC with CH_3CN-H_2O (20:80, 2.5 mL/min) to afford **1** (1.5 mg, t_R = 24.7 min), **2** (3.5 mg, t_R = 20.2 min), **3** (4.5 mg, t_R = 24.3 min), **4** (8.3 mg, t_R = 19.3 min), and **5** (7.7 mg, t_R = 34.2 min) was obtained from Fr.1.6.2 (51.8 mg) and Fr.1.6.3 (62.3 mg) by semipreparative HPLC (CH_3CN-H_2O, 25:75, 2.5 mL/min). Fr.1.8 (1.2 g) was separated by

RP-C18 preparative HPLC using MeOH/H_2O (47:53) to obtain the following fractions (Fr.1.8.1–Fr.1.8.5). Among them, Fr.1.8.4 (50.2 mg) and Fr 1.8.5 (24.5 mg) were separated by semipreparative HPLC with CH_3CN-H_2O (28:77, 2.5 mL/min) to afford **7** (7.0 mg, t_R = 11.2 min), **8** (6.2 mg, t_R = 14.7 min), **9** (11.5 mg, t_R = 16.6 min), **10** (12.0 mg, t_R = 25.4 min) and **11** (33.2 mg, t_R = 39.2 min).

1.3 NMR calculations

The conformational analysis of isolated compounds was performed on the CONFLEX software by using MMFF94s molecular force field [1]. All the conformers whose Boltzmann distribution is more than 1% were chosen, and then they were initially optimized at B3LYP/6-31G(d) level in chloroform using the polarizable continuum model (PCM) solvent model by Gaussian 09 program package [2]. The gauge independent atomic orbital (GIAO) shielding constants of these conformers were calculated at the mPW1PW91/6-311+G(d,p) level after geometry optimization. Boltzmann-weighted averages of the chemical shifts were calculated to scale them against the experimental values. The ^{1}H NMR and ^{13}C NMR chemical shift of tetramethylsilane were calculated at the same level and used as reference. The shielding constants obtained were converted into chemical shifts by referencing to TMS at 0 ppm (δcal = σTMS - σcal). The $MAE_{\Delta\Delta\delta}$ values, DP4+ and CP3 probability were calculated for evaluation of the deviations between the experimental and calculated results.

1.4 ECD calculations

Conformational analysis of all the possible conformers of isolated compounds were performed by using the MMFF94 force field in CONFLEX software. All the conformers obtained were screened based on the energy of optimized structures at the B3LYP/6-31G(d) level in an energy window of 3 kcal/mol in the Gaussian 09 software. Then, the ECD data of all the selected conformers were calculated with the time-dependent density functional theory (TDDFT) method at the B3LYP/6-311+G(2d, p) levels with the CPCM model in methanol solution. Finally, the Boltzmann-averaged ECD curve was generated using SpecDis 1.51.

1.5 NO releasing inhibition assay

The inhibition of NO production was assessed by measuring the level of nitrite (NO2−) using Griess

reaction (Li et al., 2015; Maeda et al., 2013). The RAW264.7 cells were seeded in 96-well plate (5 × 105 cells/well) overnight and then incubated with different concentrations of test compounds (3, 10, 30, 100 μM) for 40 min. After pre-incubation with LPS (10 ng/mL) at 37 °C for 24 h, the culture supernatant was transferred to the enzyme-labelled plates and mixed with an equal volume of Griess reagent. 10 min later, the absorbance was measured at 540 nm on a microplate reader. Each experiment was repeated at least three times. Fresh culture medium was used to be control group in all experiments.

1.6 COX-2 inhibitory activity

In vitro COX-2 activity assay was performed by using cyclooxygenase 2 Inhibitor Screening Kit (Beyotime, Cat No. S0168, China). COX-2 assay buffer (75 μL), COX-2 cofactor working solution (5 μL) and COX-2 working solution (5 μL) were pre-incubated with serially diluted compounds (5 μL) for 10 min at 37℃, then the COX-2 substrate (5 μL) and COX-2 probe (5 μL) were added for another 15 min incubation at 37℃. The optical density (OD) values were thereafter measured with the excitation wavelength at 560 nm and the emission wavelength at 590 nm respectively by Microplate Reader (BioTek, Synergy 2). The data were analyzed using GraphPad Prism8 (GraphPad Software Inc.). All the tests were performed in triplicates.

1.7 Molecular docking

In this study, the crystal structure of COX-2 in complex with celecoxib (PDB ID: 3LN1) was obtained from the PDB database (https://www.rcsb.org/). The structure was prepared using the Protein Preparation Wizard [3] module of Schrödinger Suite 2021-2 with default settings. This included removing water and solvent molecules, adding hydrogen atoms, completing missing side chains and loops, optimizing hydrogen bond networks, and energy minimization. To prepare the small molecule structures for docking, the LigPrep (LigPrep, Schrödinger, LLC, New York, NY, 2021) module with default settings was used to convert the 2D structures to 3D structures. The Induced Fit Docking (Induced Fit Docking, Schrödinger, LLC, New York, NY, 2021) tool was then applied to dock the target compounds to the protein by the standard protocol. The center of the docking box was placed at the position of the native ligand celecoxib, and other docking parameters were set to default values. To evaluate the reliability of the docking method, prior to docking the active compounds, the native ligand celecoxib was redocked into the active site of COX-2. The top-ranked docking pose had an RMSD of 0.8039 Å compared to the native ligand pose, indicating the accuracy of the

docking method. Next, the five active compounds in the study were docked individually into the active pocket where celecoxib binds to explore potential modes of interaction between the small molecules and the protein. Finally, the simulation results were analyzed and visualized using the Maestro (Maestro, Schrödinger, LLC, New York, NY, 2021) of Schrödinger and Pymol (The PyMOL Molecular Graphics System, Version 2.3 Schrödinger, LLC).

1.8 Molecular dynamics simulation

Binding Pose Metadynamics is an enhanced sampling method that allows for the evaluation of the binding stability of small molecule ligands to proteins in aqueous solutions within a short simulation time. In this study, we utilized Schrödinger's Binding Pose Metadynamics tool to investigate the stability of compounds **3** and **4** while binding to the COX-2 active site in an aqueous solution. The simulation parameters were set to their default values, with the exception of the number of trials per pose, which was set to 10.

The OLPS4 force field [4] in Desmond [5,6] software was used to simulate the compound **3**/COX-2 and compound **4**/COX-2 complexes. These complexes were dissolved in a cubic simulation box with periodic boundary conditions. The box boundaries were set to be 10 Å away from the complexes, and K^+ and Cl^- ions were placed in the water phase to achieve an experimental salt concentration of 0.15 M KCl and neutralize the system. To ensure the accuracy of the simulation, the entire system underwent equilibration using a default protocol consisting of a series of restrained minimizations and MD simulations before the final production [7]. A 100 ns unconstrained production run was then performed using the NPT ensemble (constant number of atoms *N*, pressure *P*, and temperature *T*), resulting in 1000 frames. The particle mesh Ewald (PME) method [8,9] was used to calculate long-range electrostatic interactions, with van der Waals forces set to a cutoff of 9 Å. The Nose-Hoover chain thermostat and Martyna-Tobias-Klein barostat were used to maintain the temperature and pressure at 310K and 1.01325 bar, respectively. To analyze the trajectories, the Simulation Interaction Diagram tool was used to perform RMSD analysis of protein backbone atoms and ligand heavy atoms, as well as to analyze protein-ligand interactions. Principal component analysis was performed on the trajectories using Schrödinger's trj_essential_dynamics script, and the free energy landscape was plotted using the gmx sham command in GROMACS (V. 2022.1) [10,11] based on PC1 and PC2 of protein Cα motion, with the temperature set to 310 K used in the MD simulation. Additionally, the Schrödinger-provided thermal_mmgbsa.py script was used to calculate the binding free energy of compounds 19 and 21 to COX-2.

1.9 Cell culture

Hep3B, HepG2 cell lines were obtained from the America Type Culture Collection (USA). The cells were cultured in Dulbecco's modified eagle medium (DMEM) (Hyclone, USA) supplemented with 10% fetal bovine serum (Biological Industries, Israel) in 37 °C, 5% CO_2 incubator.

1.10 Cytotoxic activities

Cytotoxic activities of isolated sesquiterpenes against Hep3B and HepG2 cells were evaluated using an MTT assay. The cells were treated with different concentrations of each compound or DMSO. After 48 h, 20 μL MTT (5 mg/mL) was added to each well and incubated for 4 h at 37 °C. The medium was removed and DMSO (150 μL/well) was added to each well, and cell viability was measured using a microplate reader (Thermo, Carlsbad, CA, USA) at 490 nm. All tests needed three separate experiments. The IC_{50} values were calculated using GraphPad Prism 6 software.

References

[1] Bruhn, T.; Schaumlöffel, A.; Hemberger, Y.; Bringmann, G. SpecDis: quantifying the comparison of calculated and experimental electronic circular dichroism spectra. Chirality *25* (2013) 243–249.

[2] Frisch, M. J.; Trucks, G. W.; Schlegel, H. B.; Scuseria, G. E.; Robb, M. A.; Cheeseman, J. R.; Scalmani, G.; Barone, V.; Mennucci, B.; Petersson, G. A.; Nakatsuji, H.; Caricato, M.; Li, X.; Hratchian, H. P.; Izmaylov, A. F.; Bloino, J.; Zheng, G.; Sonnenberg, J. L.; Hada, M.; Ehara, M.; Toyota, K.; Fukuda, R.; Hasegawa, J.; Ishida, M.; Nakajima, T.; Honda, Y.; Kitao, O.; Nakai, H.; Vreven, T.; Montgomery, Jr, J. A.; Peralta, J. E.; Ogliaro, F.; Bearpark, M.; Heyd, J. J.; Brothers, E.; Kudin, K. N.; Staroverov, V. N.; Keith, T.; Kobayashi, R.; Normand, J.; Raghavachari, K.; Rendell, A.; Burant, J. C.; Iyengar, S. S.; Tomasi, J.; Cossi, M.; Rega, N.; Millam, J. M.; Klene, M.; Knox, J. E.; Cross, J. B.; Bakken, V.; Adamo, C.; Jaramillo, J.; Gomperts, R.; Stratmann, R. E.; Yazyev, O.; Austin, A. J.; Cammi, R.; Pomelli, C.; Ochterski, J. W.; Martin, R. L.; Morokuma, K.; Zakrzewski, V. G.; Voth, G. A.; Salvador, P.; Dannenberg, J. J.; Dapprich, S.; Daniels, A. D.; Farkas, O.; Foresman, J. B.; Ortiz, J. V.; Cioslowski, J.; Fox, D. J. Gaussian 09, Revision D.01. *Gaussian, Inc., Wallingford*, *CT*, 2013.

[3] G. M. Sastry, M. Adzhigirey, T. Day, R. Annabhimoju, W. Sherman, Protein and ligand preparation: parameters, protocols, and influence on virtual screening enrichments. J. Comput. Aided Mol. Des. 27 (2013) 221–234.

[4] C. Lu, C. J. W, D. Ghoreishi, et al. OPLS4: Improving force field accuracy on challenging regimes of chemical apace. J. Chem. Theory Comput. 17 (2021) 4291–4300.

[5] Desmond, Desmond Molecular Dynamics System, D. E. Shaw Research, New York, NY, (2021). Maestro-Desmond

Interoperability Tools, Schrödinger, New York, NY, (2021).
[6] K. J. Bowers, Chow, D. E., Xu, H., Dror, R. O., Eastwood, M. P., Gregersen, B. A., et al. Scalable algorithms for molecular dynamics simulations on commodity clusters. SC '06: proceedings of the 2006 ACM/IEEE conference on supercomputing pp 43–43 (2006).
[7] F. M. He, X. M. Wang, Q. Q. Wu, Identification of potential ATP-competitive cyclin-dependent kinase 1 inhibitors: De novo drug generation, molecular docking, and molecular dynamics simulation. Comput. Biol. Med. 155 (2023) 106645.
[8] A. Toukmaji, C. Sagui, J. A. Board, T. A. Darden, Efficient particle-mesh Ewald based approach to fixed and induced dipolar interactions. J. Chem. Phys. 113 (2000) 10913–10927.
[9] T. Darden, D. York, L. Pedersen, Particle mesh Ewald: An N·log(N) method for Ewald sums in large systems. J. Chem. Phys. 98 (1993) 10089–10092.
[10] M. J. Abraham et al., GROMACS: High performance molecular simulations through multi-level parallelism from laptops to supercomputers. SoftwareX 1–2 (2015) 19–25.
[11] D. Van Der Spoel et al., GROMACS: Fast, flexible, and free. J. Comput. Chem. 26 (2005) 1701–1718.

2. Supplementary 2

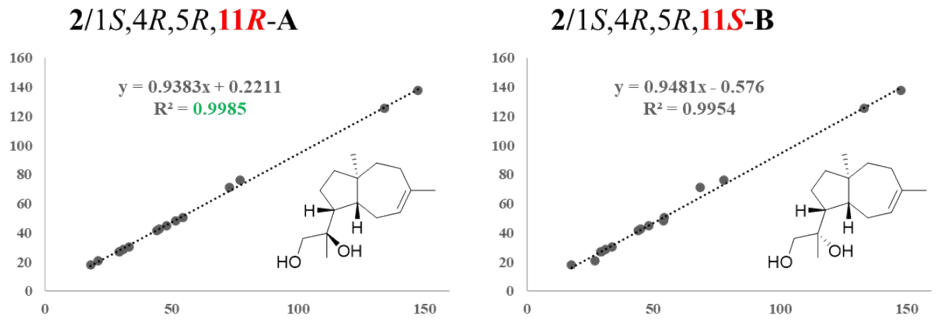

DP4+ calculation Probabilities:

Number/isomers	A	B
2	**100.0%**	0.0%

Figure S1. The relative configurations determination of **2** by R^2 and DP4+ analysis.

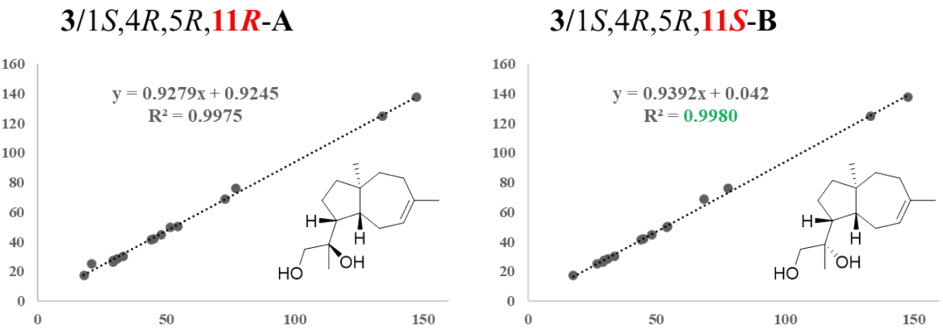

DP4+ calculation Probabilities:

Number/isomers	A	B
3	0.0%	**100%**

Figure S2. The relative configurations determination of **3** by R^2 and DP4+ analysis.

CP3 calculation Probabilities:

	C data	H data	All data
Exp_**2**-Cal_**A** & Exp_**3**-Cal_**B**	**100.0%**	**100.0%**	**100.0%**
Exp_**2**-Cal_**B** & Exp_**3**-Cal_**A**	0.0%	0.0%	0.0%

MAE$_{\Delta\Delta\delta}$ parameter:

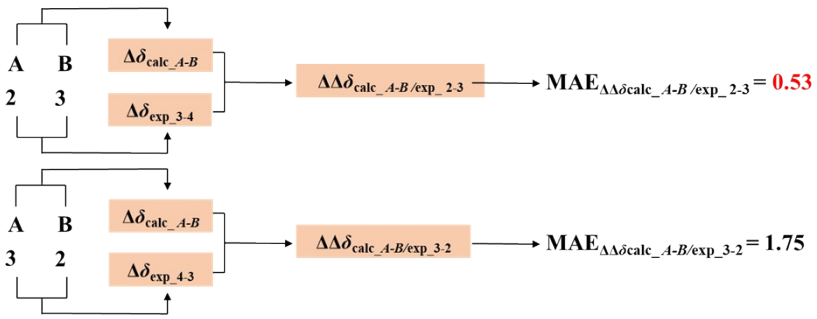

Figure S3. The relative configurations determination of **2** and **3** by MAE$_{\Delta\Delta\delta}$ and CP3 analysis.

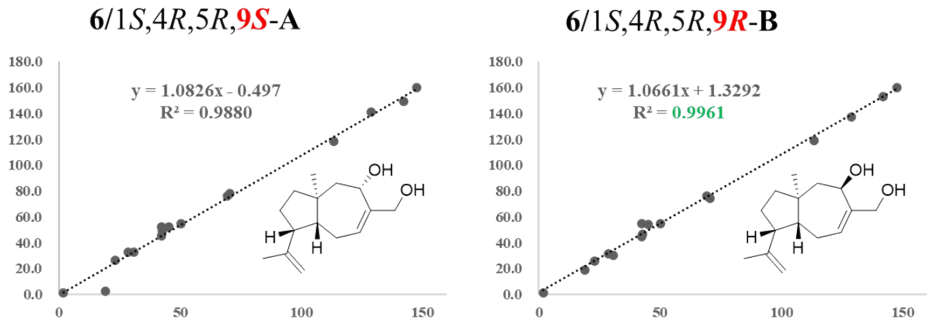

DP4+ calculation Probabilities:

Number/isomers	A	B
6	0.0%	**100.0%**

Figure S4. The relative configurations determination of **6** by R^2 and DP4+ analysis.

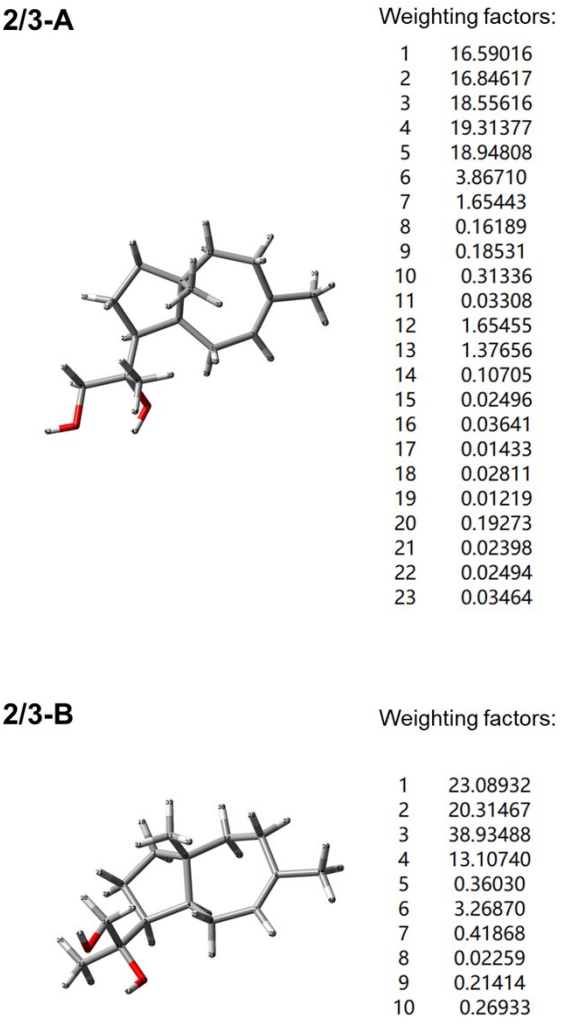

Figure S5. The weighting factors of structures **2/3-A and 2/3-B** for NMR calculation.

	2	3		A	B
1	42.4	42.1	1	45.2	44.9
2	26.8	26.2	2	29.3	29.3
3	48.1	49.8	3	51.6	54.1
4	50.7	50.4	4	54.5	54.2
5	44.6	44.6	5	48.0	48.1
6	26.9	27.6	6	29.4	29.4
7	125.4	124.7	7	134.1	133.5
8	137.5	137.6	8	147.5	147.9
9	30.4	30.4	9	33.3	33.5
10	41.3	41.3	10	44.2	44.1
11	17.9	17.5	11	18.0	17.7
12	76.2	76	12	77.2	78.0
13	21	25	13	21.0	26.8
14	71	68.8	14	72.8	68.5
15	28.5	28.5	15	30.9	31.0
18	1.45	1.45	18	1.44	1.35
19	1.32	1.32	19	1.33	1.27
20	1.62	1.68	20	1.43	1.53
21	1.31	1.54	21	1.25	1.34
22	2.45	2.44	22	2.35	2.34
23	1.91	1.85	23	1.82	1.71
24	2.77	2.55	24	3.03	3.16
25	2.15	2.07	25	2.22	2.15
26	5.51	5.46	26	5.98	5.96
27	1.89	1.89	27	1.86	1.80
28	2.25	2.21	28	2.36	2.34
29	1.25	1.24	29	1.19	1.12
30	1.67	1.66	30	1.59	1.58
31	0.88	0.84	31	0.89	0.78
32	0.88	0.84	32	0.89	0.78
33	0.88	0.84	33	0.89	0.78
34	1.19	1.26	34	1.09	1.12
35	1.19	1.26	35	1.09	1.12
36	1.19	1.26	36	1.09	1.12
37	3.4	3.61	37	3.29	3.62
38	3.28	3.49	38	3.16	3.47
39	1.7	1.69	39	1.77	1.78
40	1.7	1.69	40	1.77	1.78
41	1.7	1.69	41	1.77	1.78

Figure S6. Calculated ^{13}C NMR chemical shifts of two candidate structures (**A**-**B**-**2**/**3**)

1 2	2 3	Δδexp1-2	Δδexp2-1	A	B	ΔδcalcA-B
42.4	42.1	0.3	-0.3	45.23389	44.87251	0.36138
26.8	26.2	0.6	-0.6	29.26103	29.29642	-0.03539
48.1	49.8	-1.7	1.7	51.56225	54.05787	-2.49562
50.7	50.4	0.3	-0.3	54.47373	54.22769	0.24604
44.6	44.6	0	0	48.01401	48.05152	-0.03751
26.9	27.6	-0.7	0.7	29.44981	29.40908	0.04073
125.4	124.7	0.7	-0.7	134.07495	133.49199	0.58296
137.5	137.6	-0.1	0.1	147.54969	147.91203	-0.36234
30.4	30.4	0	0	33.31283	33.53201	-0.21918
41.3	41.3	0	0	44.18437	44.13517	0.0492
17.9	17.5	0.4	-0.4	17.98244	17.68752	0.29492
76.2	76	0.2	-0.2	77.23448	78.00465	-0.77017
21	25	-4	4	21.02985	26.84963	-5.81978
71	68.8	2.2	-2.2	72.75429	68.45963	4.29466
28.5	28.5	0	0	30.88507	31.00766	-0.12259

ΔΔδcalcA-B/exp1-2		ΔΔδcalcA-B/exp2-1	
0.06138	0.06138	0.66138	0.66138
-0.63539	0.63539	0.56461	0.56461
-0.79562	0.79562	-4.19562	4.19562
-0.05396	0.05396	0.54604	0.54604
-0.03751	0.03751	-0.03751	0.03751
0.74073	0.74073	-0.65927	0.65927
-0.11704	0.11704	1.28296	1.28296
-0.26234	0.26234	-0.46234	0.46234
-0.21918	0.21918	-0.21918	0.21918
0.0492	0.0492	0.0492	0.0492
-0.10508	0.10508	0.69492	0.69492
-0.97017	0.97017	-0.57017	0.57017
-1.81978	1.81978	-9.81978	9.81978
2.09466	2.09466	6.49466	6.49466
-0.12259	0.12259	-0.12259	0.12259

MAEΔΔδcalcA-B/exp1-2
0.538975333

MAEΔΔδcalcA-B/exp2-1
1.758682

Figure S7. $MAE_{\Delta\Delta\delta}$ parameter between the experimental and calculated ^{13}C NMR chemical shifts between **2/3** and **A/B**

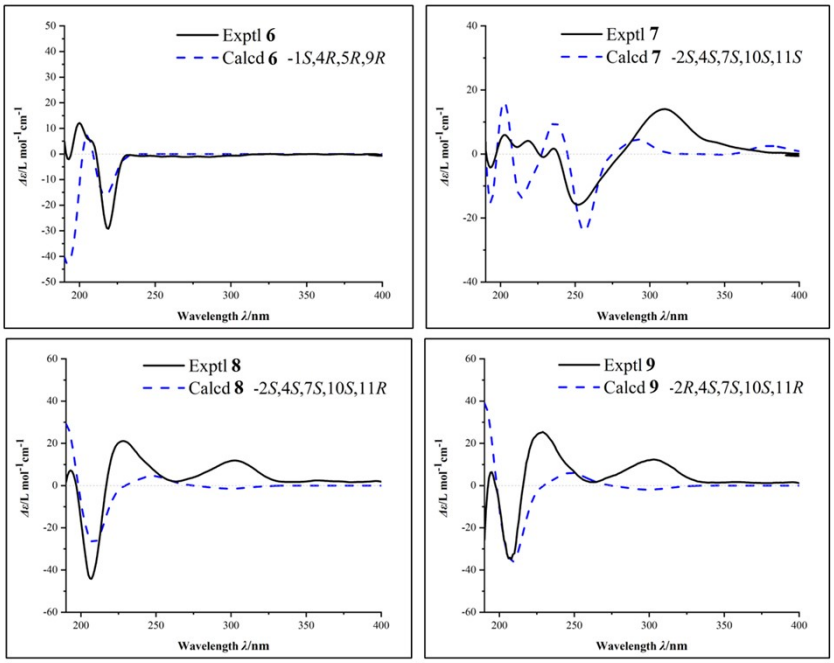

Figure S8 The calculated ECD and experimental spectra of **6-9**.

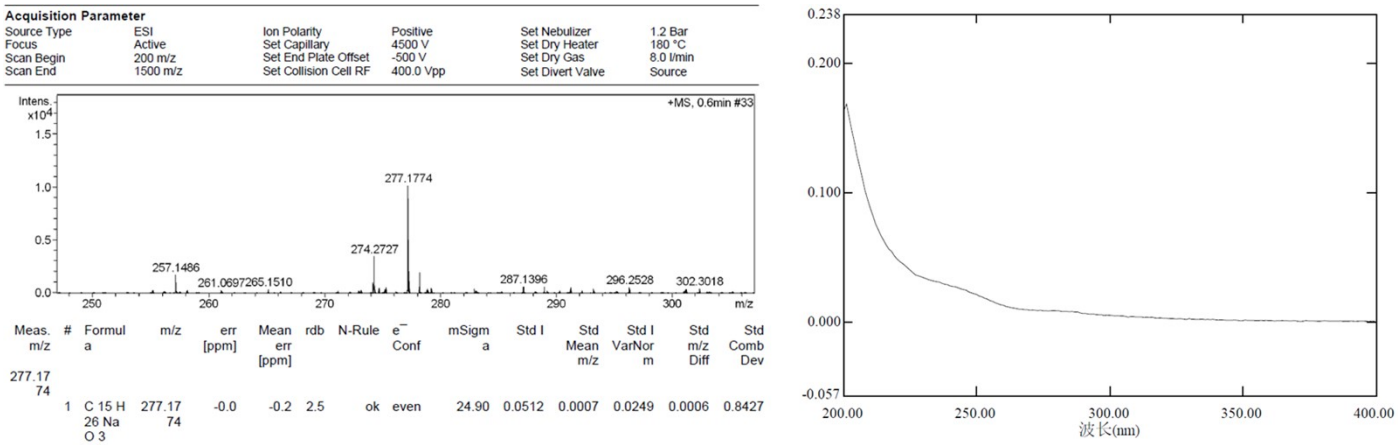

Figure S9 HRESIMS and UV spectra of compound **1**

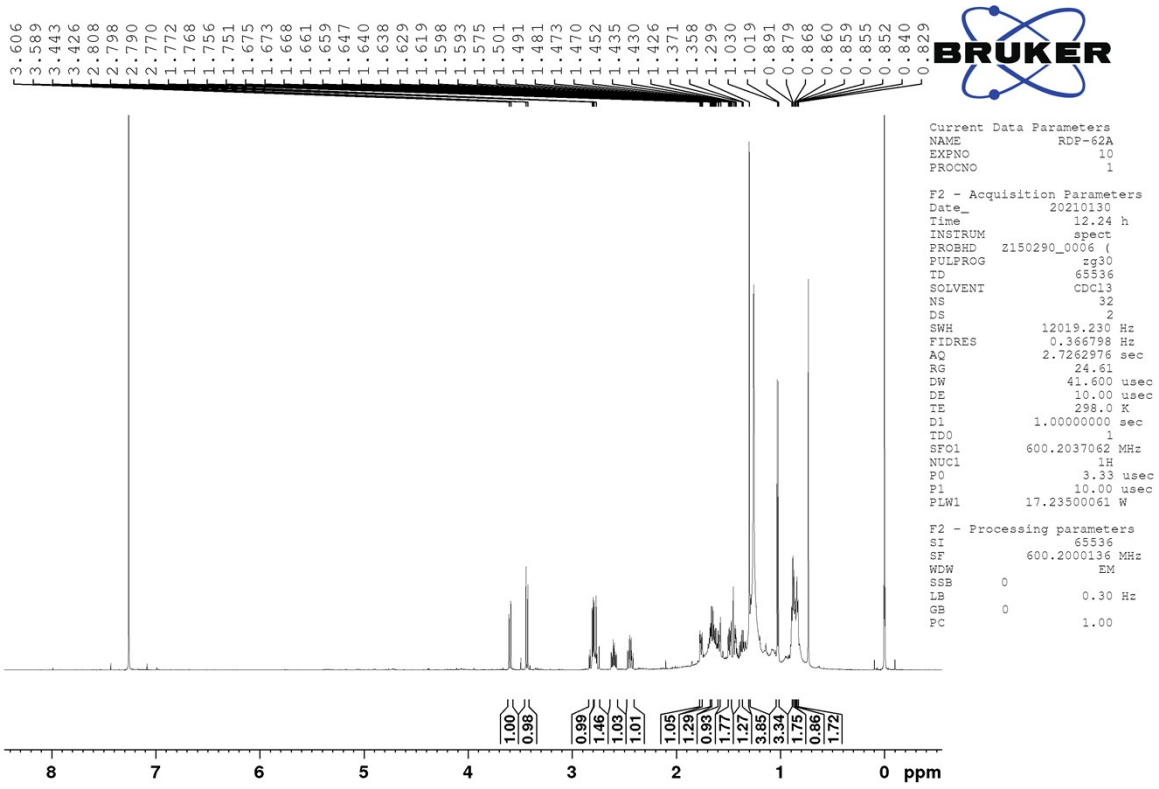

Figure S10 ^{1}H NMR spectrum (600 MHz, $CDCl_3$) of compound **1**

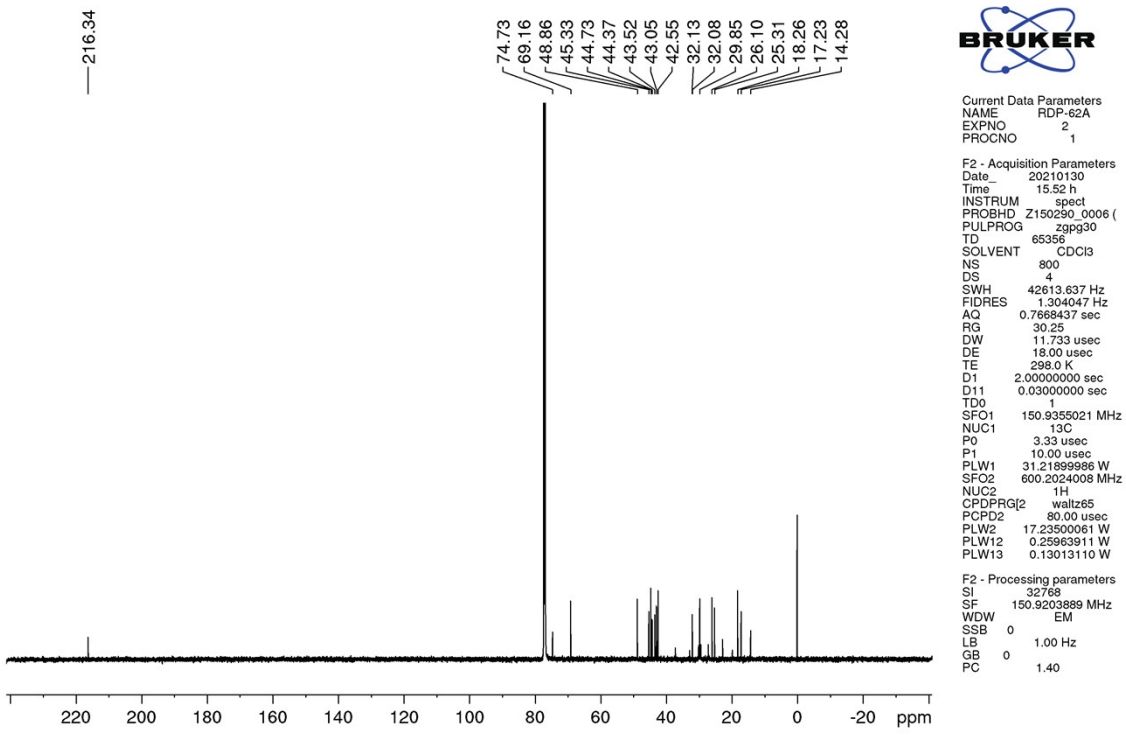

Figure S11 ^{13}C NMR spectrum (150 MHz, $CDCl_3$) of compound **1**

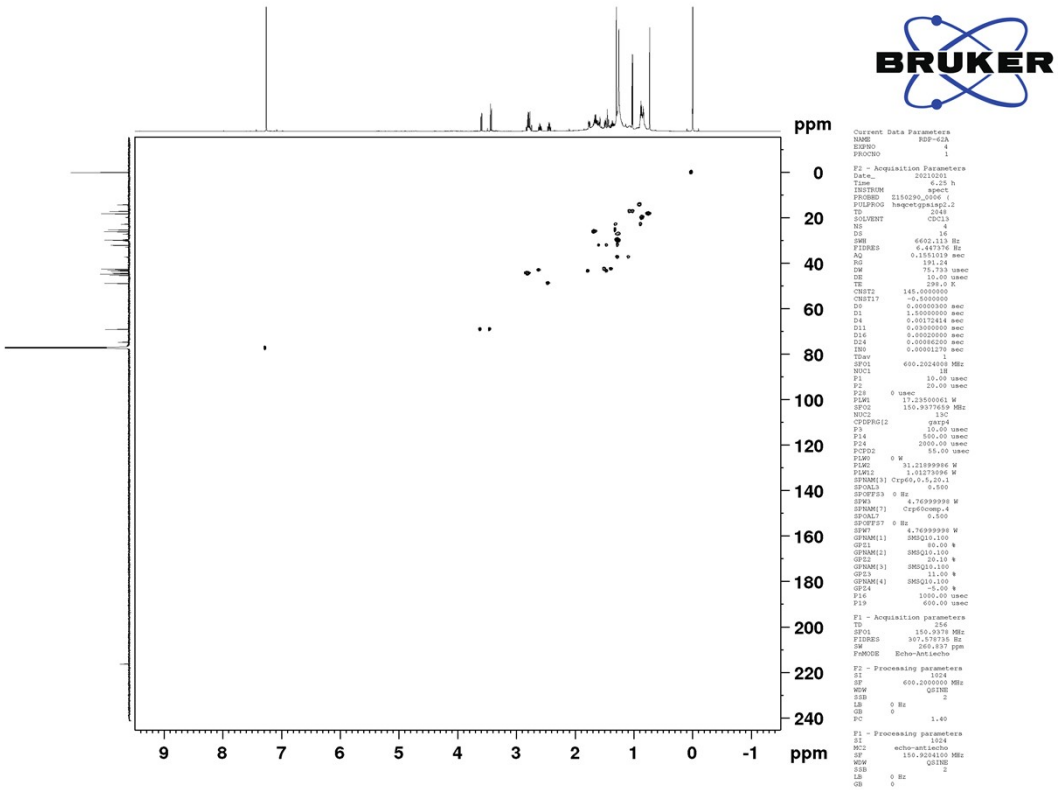

Figure S12 HSQC spectrum (600 MHz, $CDCl_3$) of compound **1**

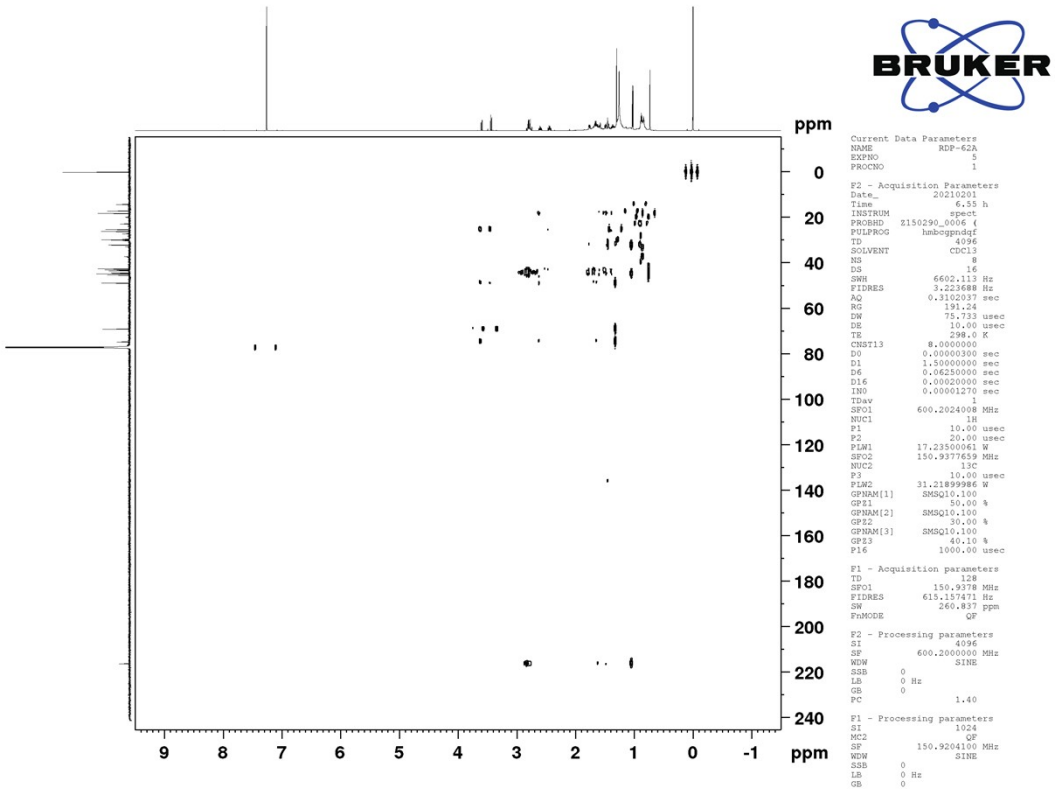

Figure S13 HMBC spectrum (600 MHz, $CDCl_3$) of compound **1**

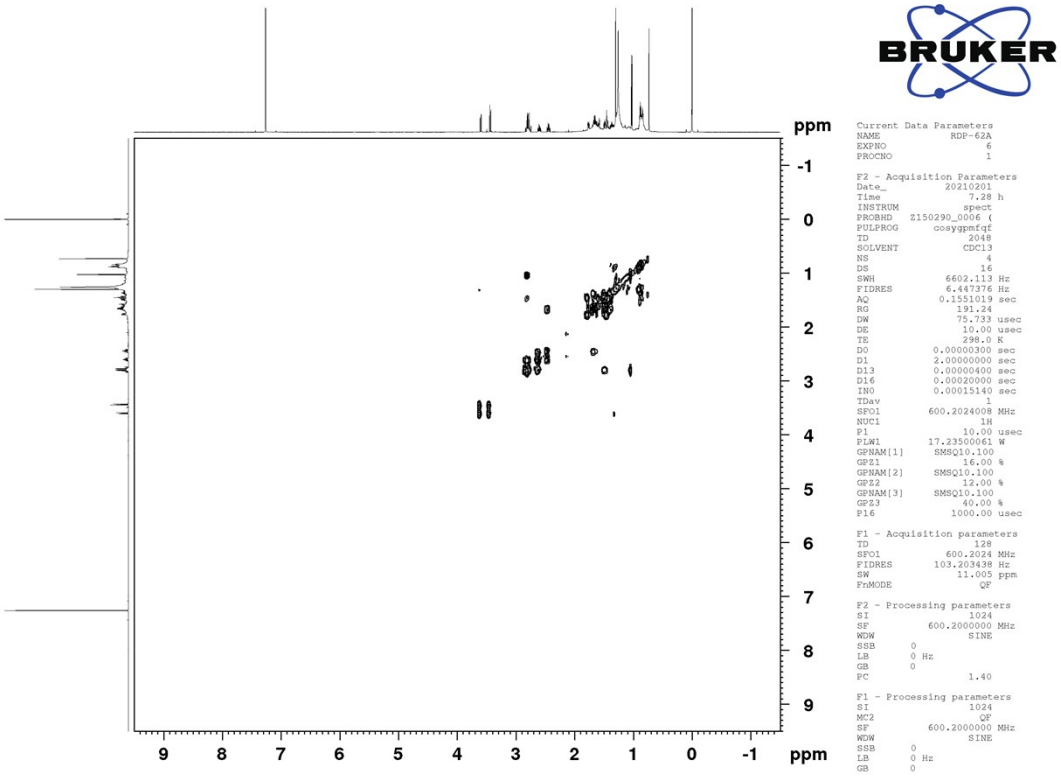

Figure S14 ^1H-^1H COSY spectrum (600 MHz, $CDCl_3$) of compound **1**

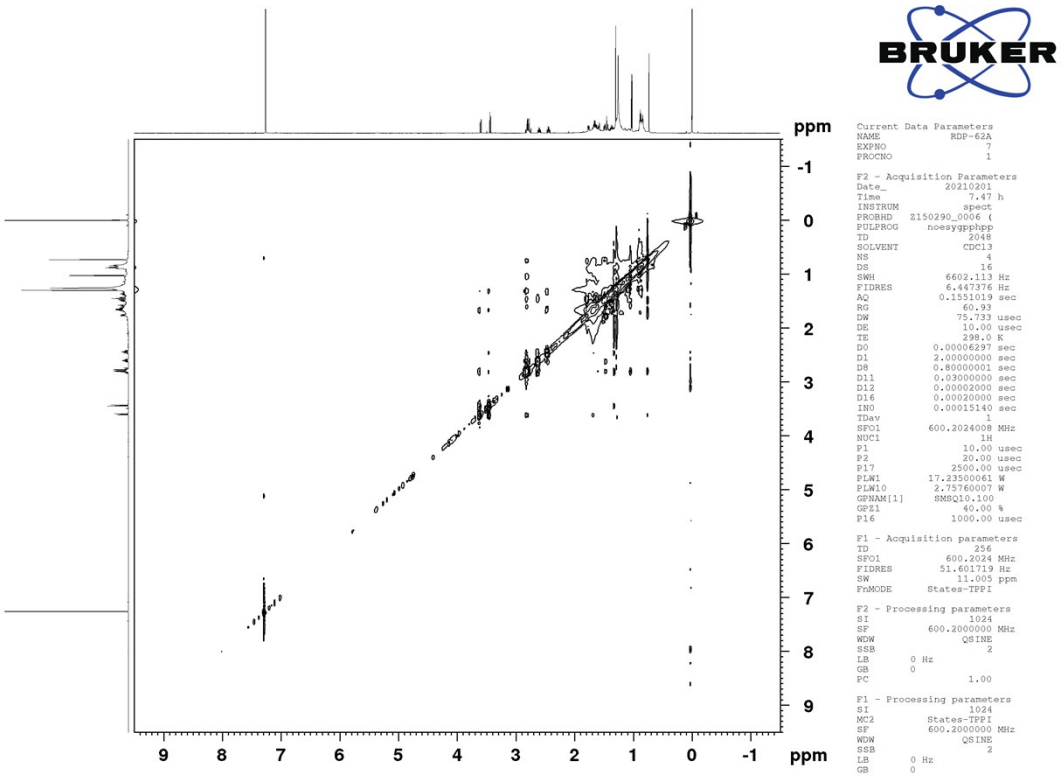

Figure S15 NOESY spectrum (600 MHz, $CDCl_3$) of compound **1**

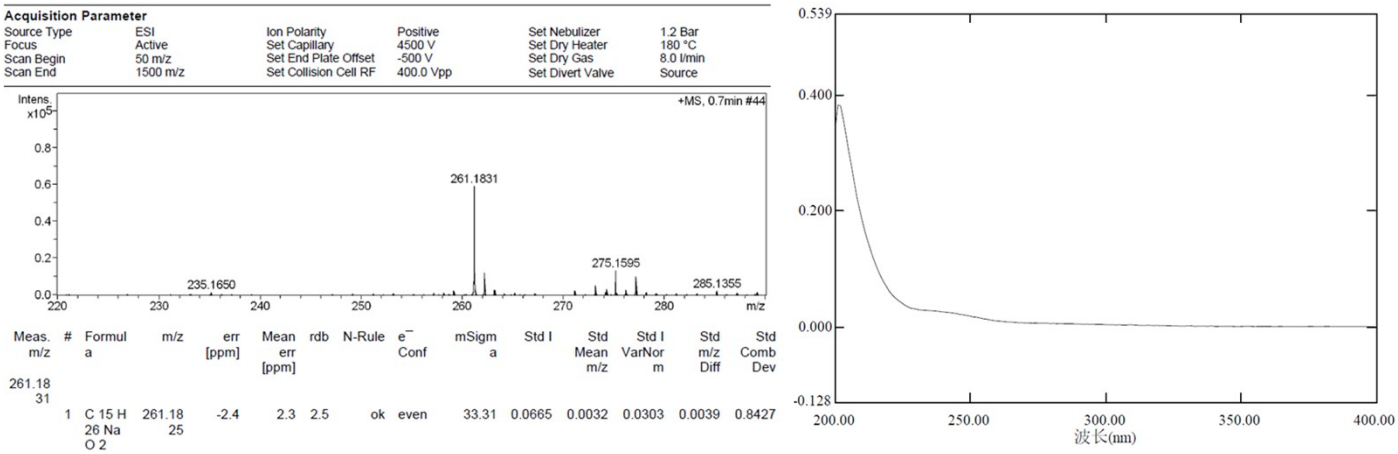

Figure S16 HRESIMS and UV spectra of compound **2**

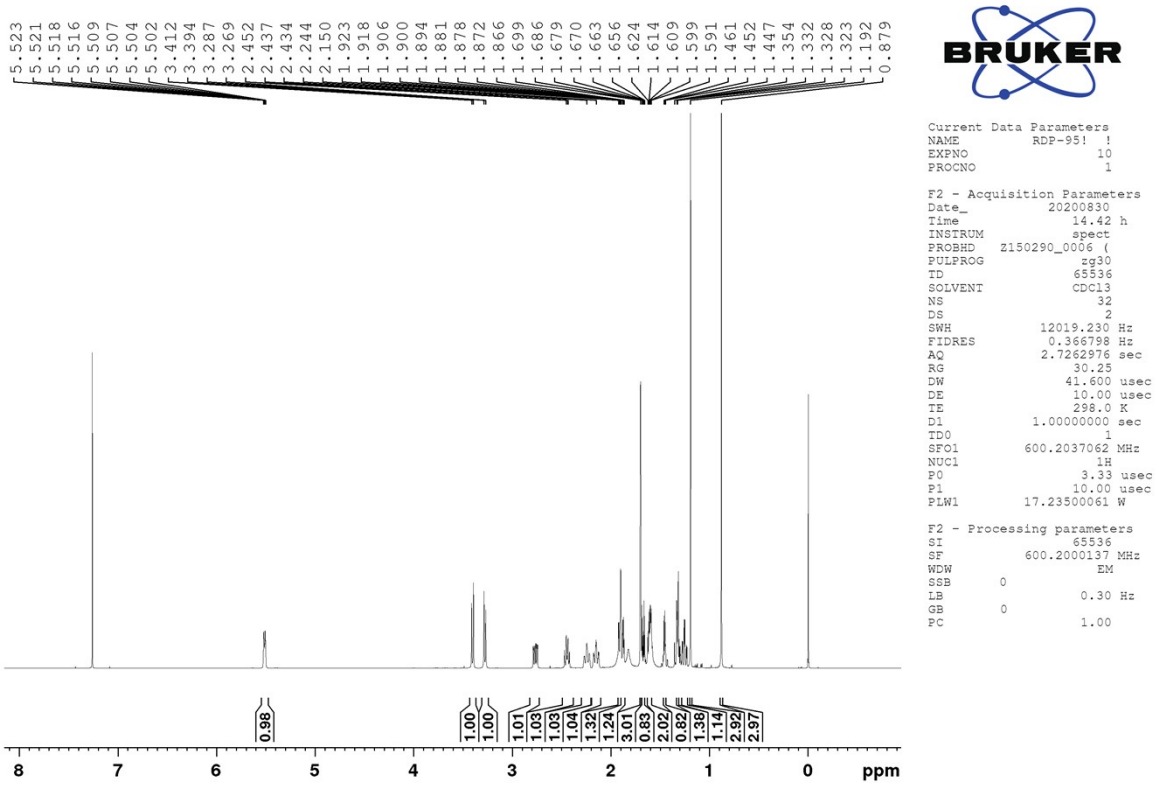

Figure S17 ^{1}H NMR spectrum (600 MHz, $CDCl_3$) of compound **2**

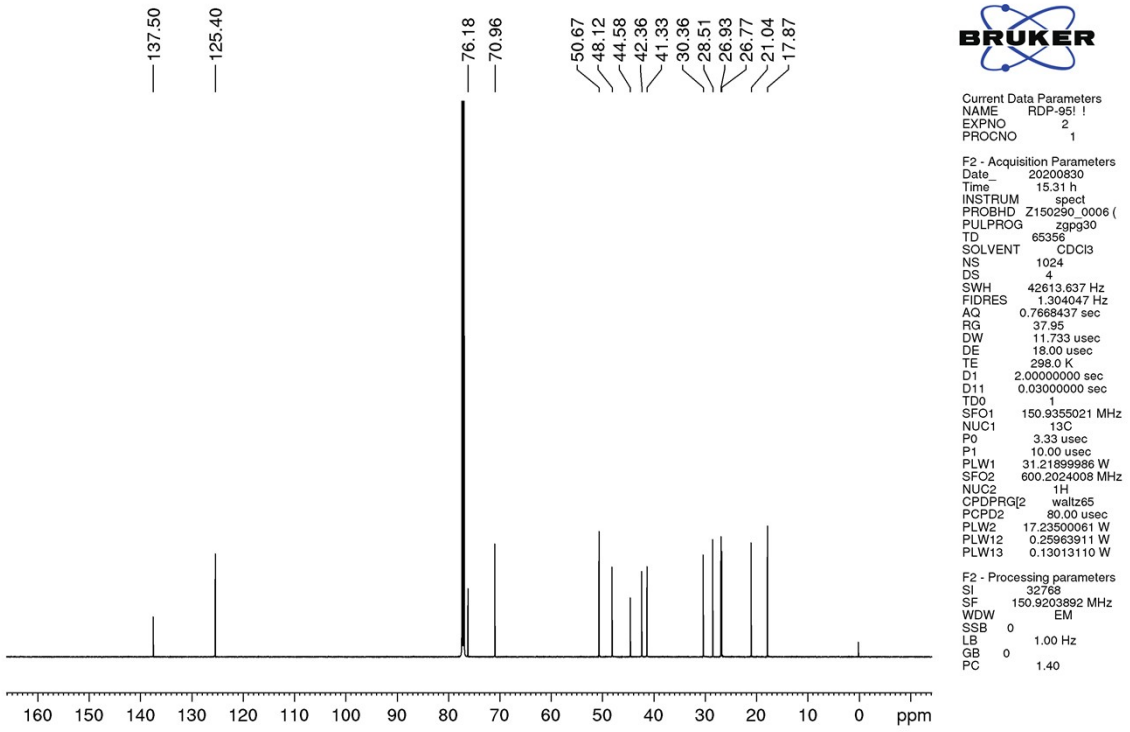

Figure S18 ^{13}C NMR spectrum (150 MHz, $CDCl_3$) of compound **2**

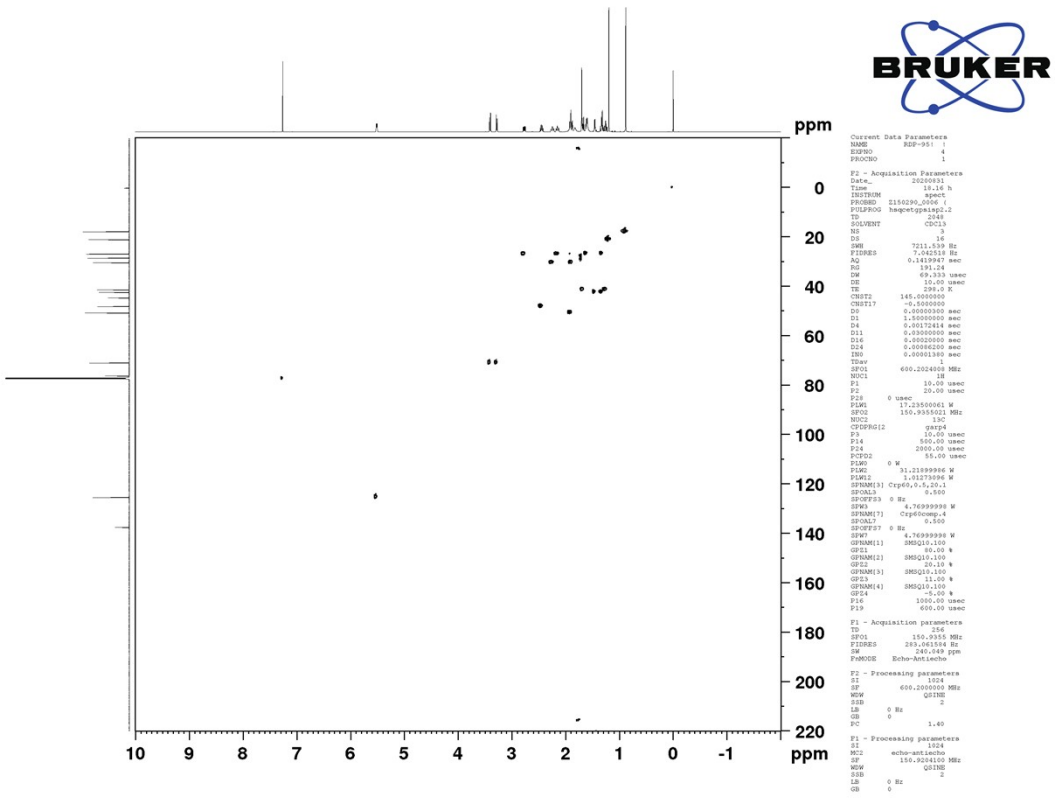

Figure S19 HSQC spectrum (600 MHz, $CDCl_3$) of compound **2**

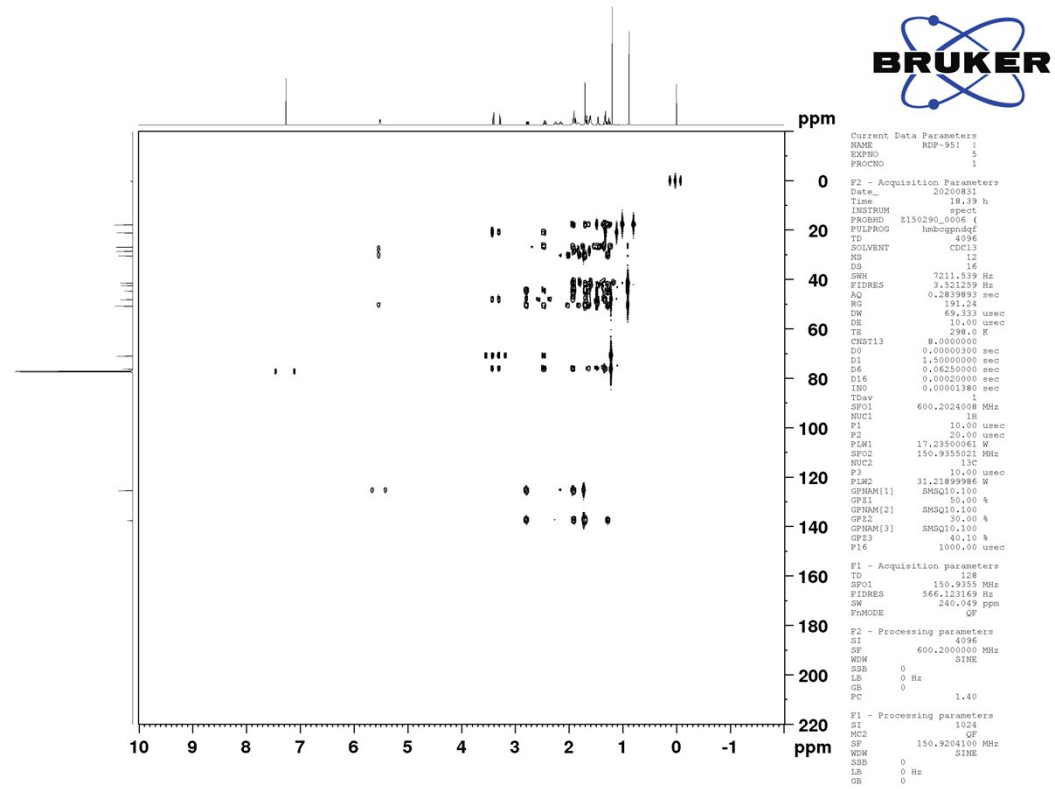

Figure S20 HMBC spectrum (600 MHz, $CDCl_3$) of compound **2**

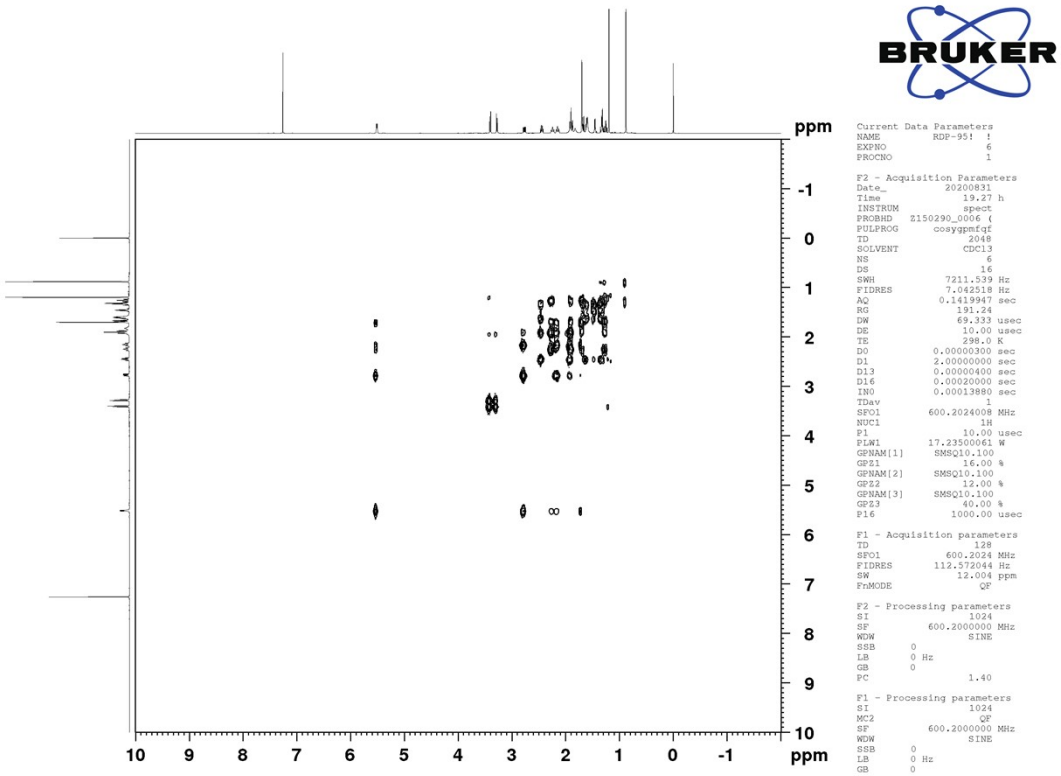

Figure S21 ^{1}H-^{1}H COSY spectrum (600 MHz, $CDCl_3$) of compound **2**

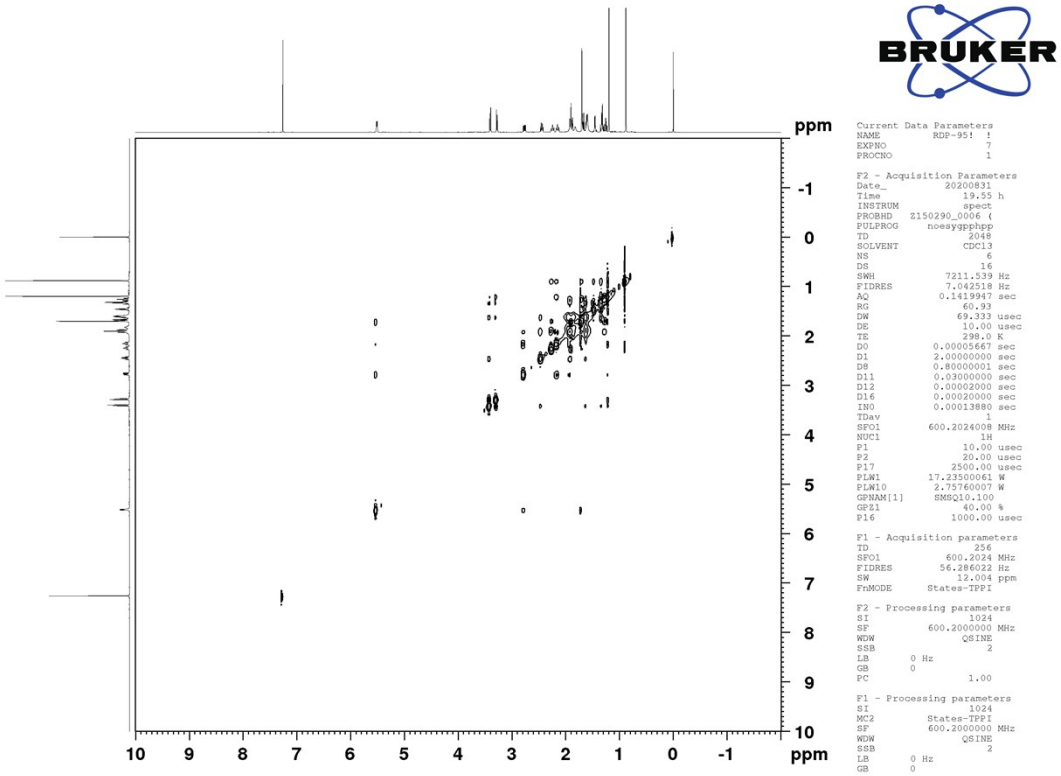

Figure S22 NOESY spectrum (600 MHz, $CDCl_3$) of compound **2**

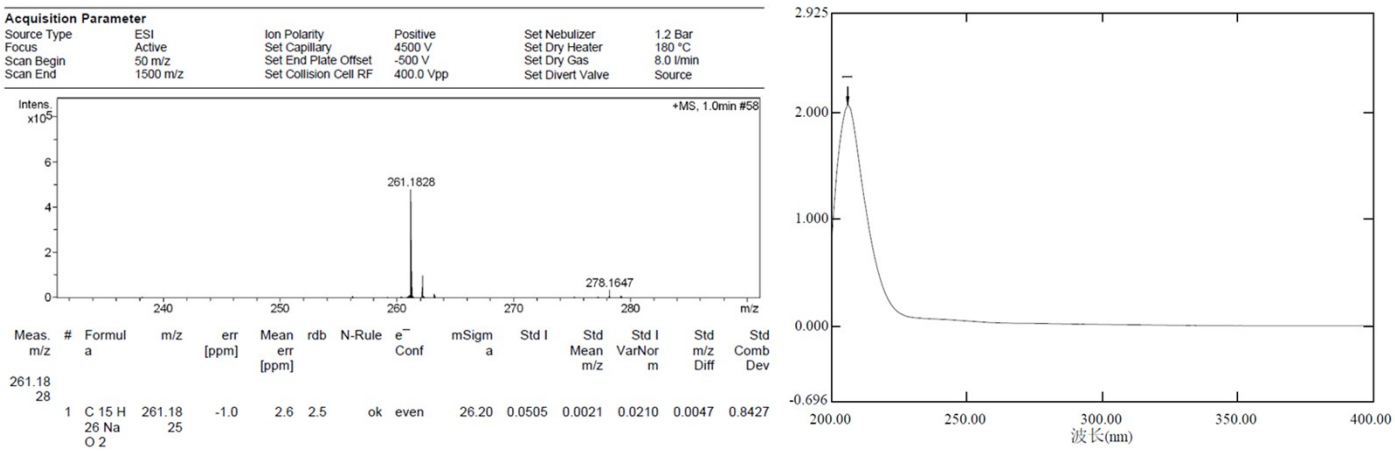

Figure S23 HRESIMS and UV spectra of compound **3**

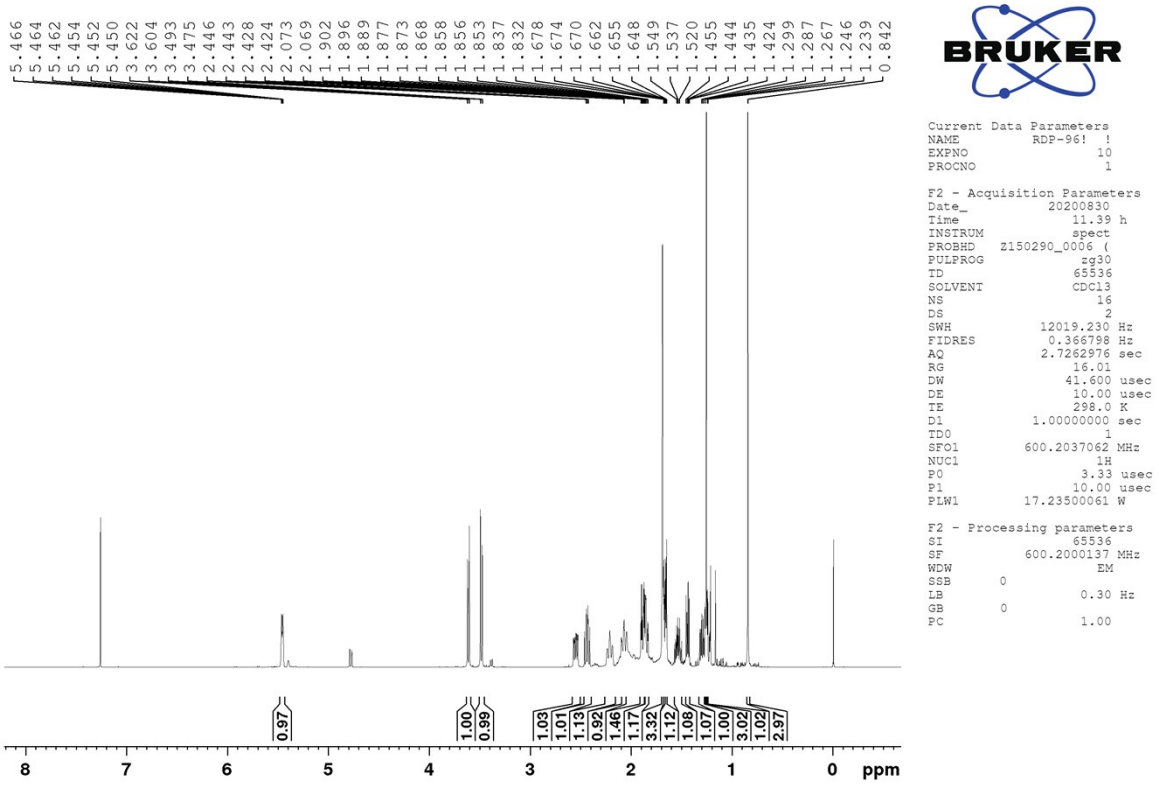

Figure S24 ^{1}H NMR spectrum (600 MHz, $CDCl_3$) of compound **3**

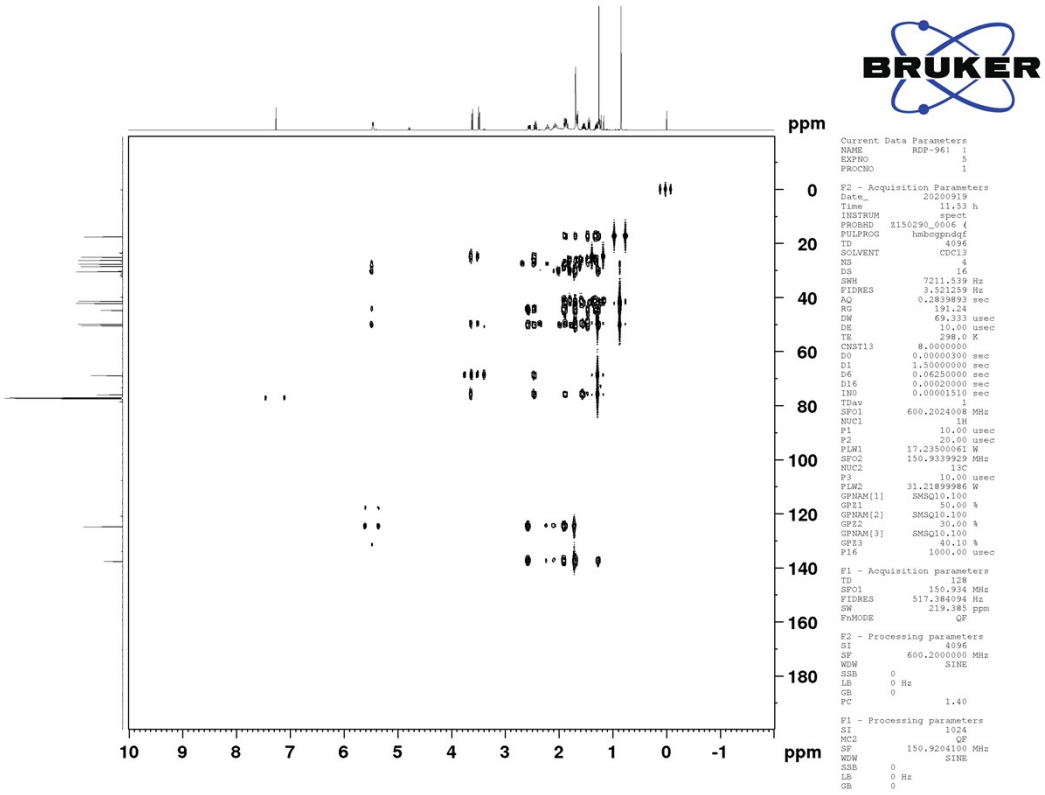

Figure S25 ^{13}C NMR spectrum (150 MHz, $CDCl_3$) of compound **3**

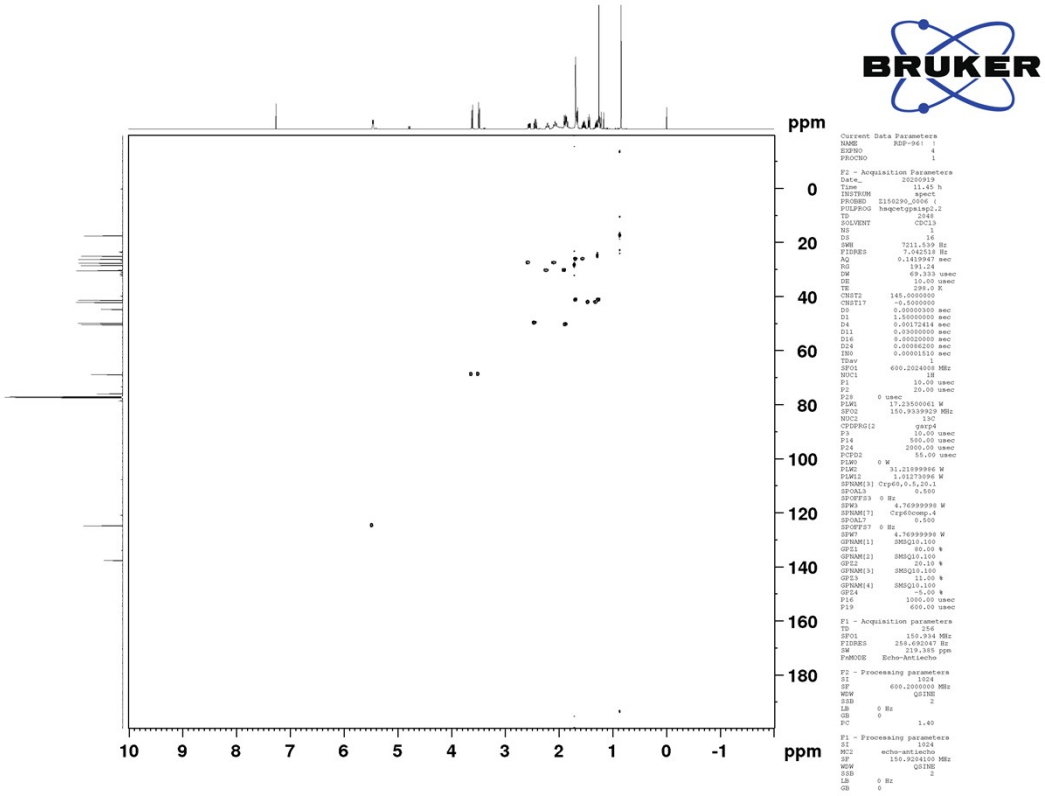

Figure S26 HSQC spectrum (600 MHz, $CDCl_3$) of compound **3**

Figure S27 HMBC spectrum (600 MHz, $CDCl_3$) of compound **3**

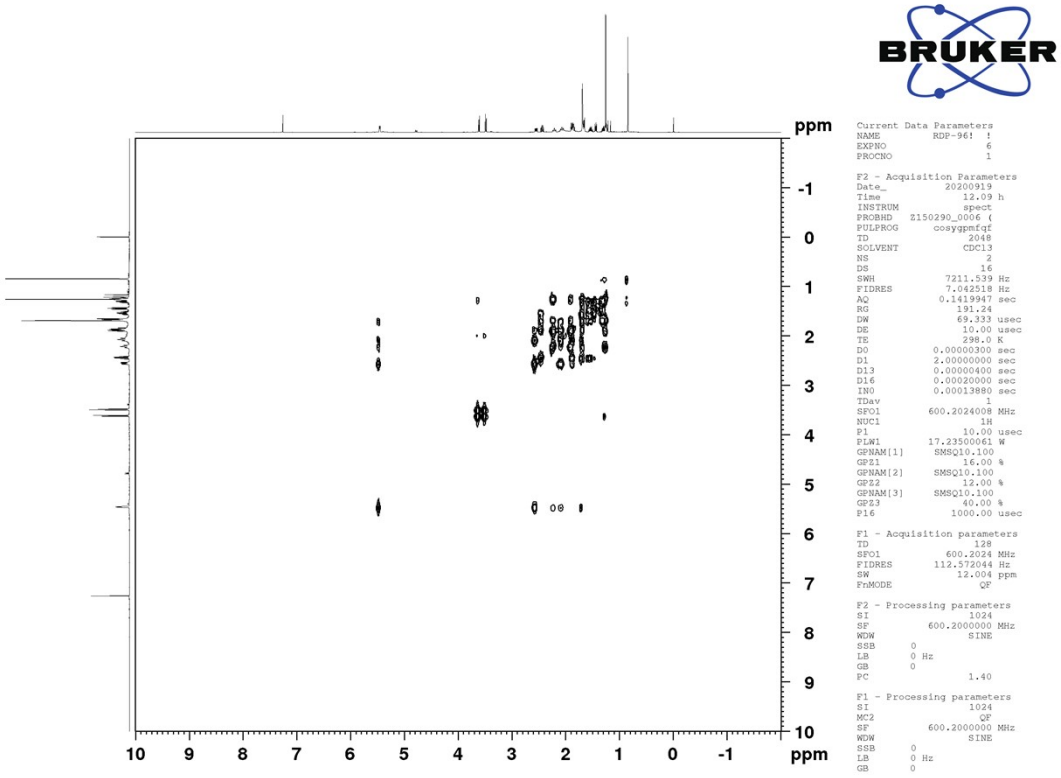

Figure S28 ^1H-^1H COSY spectrum (600 MHz, $CDCl_3$) of compound **3**

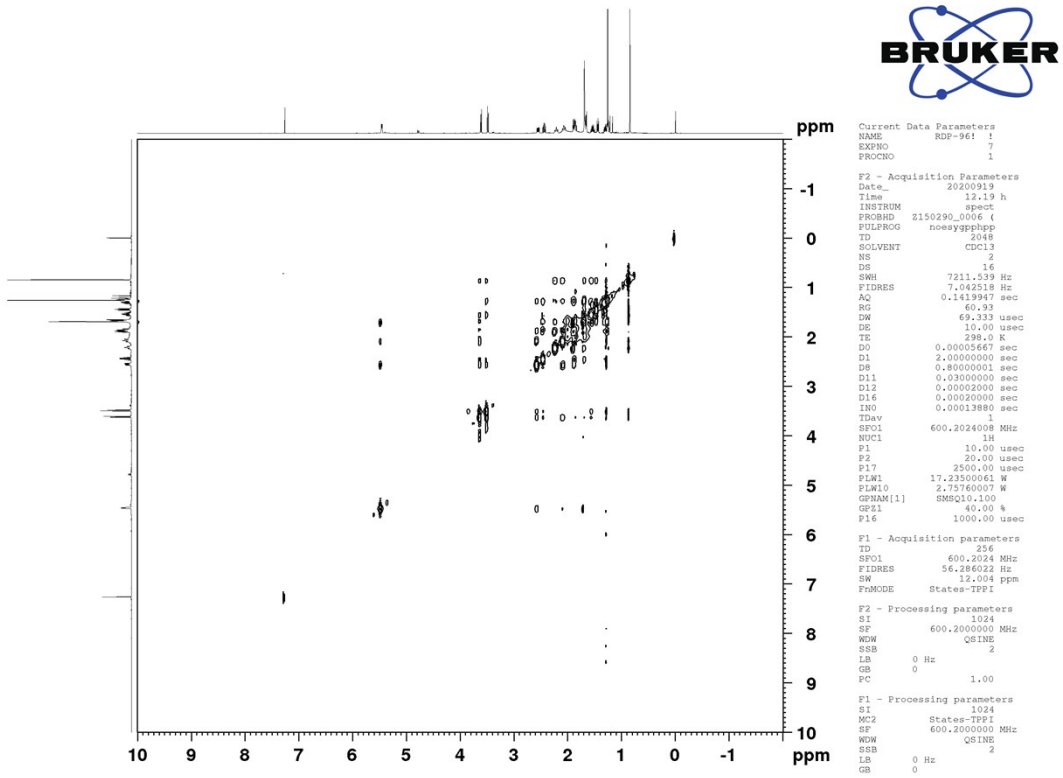

Figure S29 NOESY spectrum (600 MHz, $CDCl_3$) of compound **3**

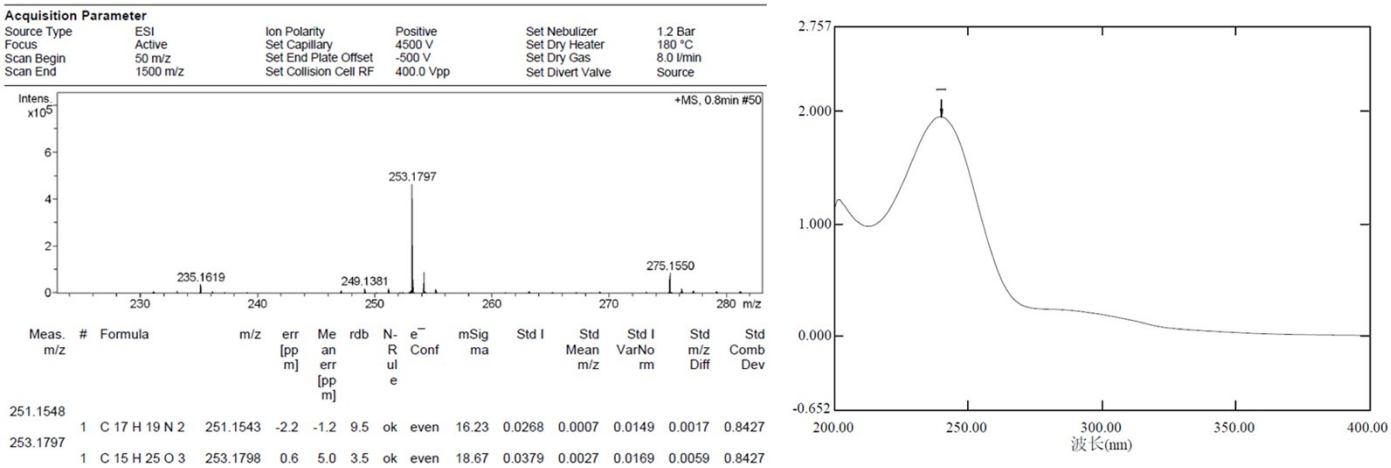

Figure S30 HRESIMS and UV spectra of compound **4**

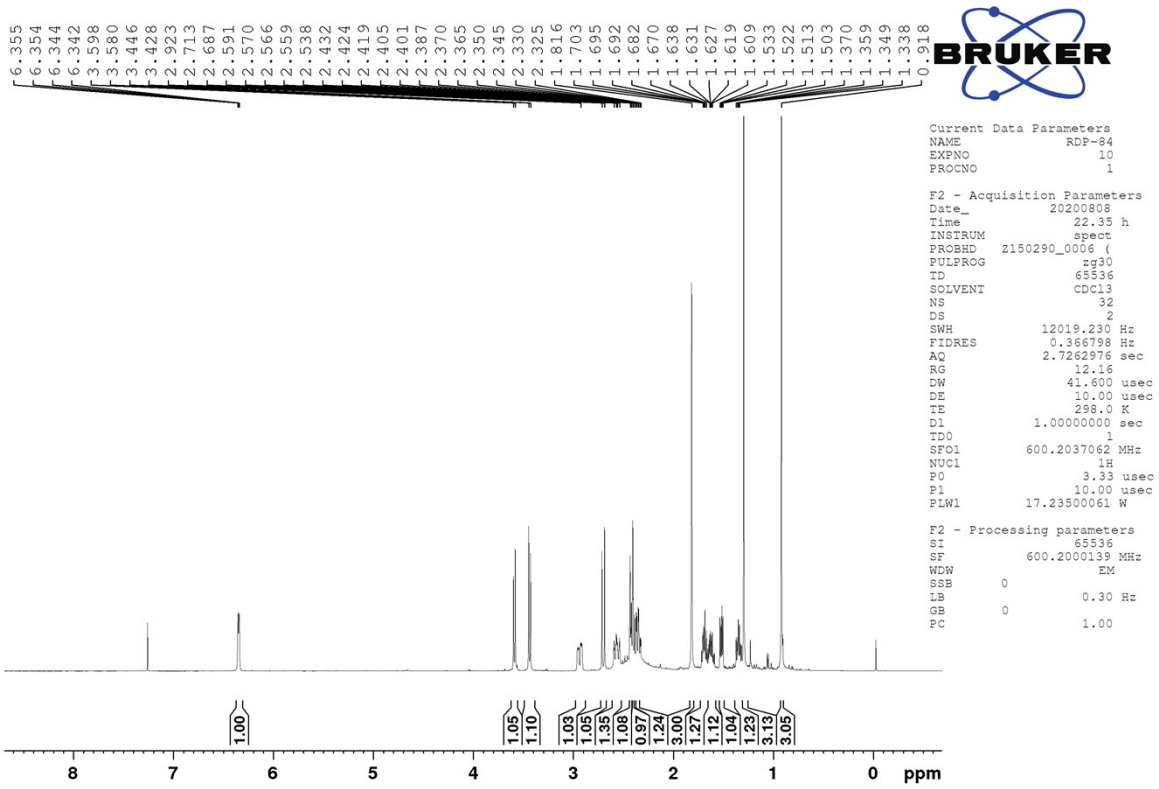

Figure S31 ^{1}H NMR spectrum (600 MHz, $CDCl_3$) of compound **4**

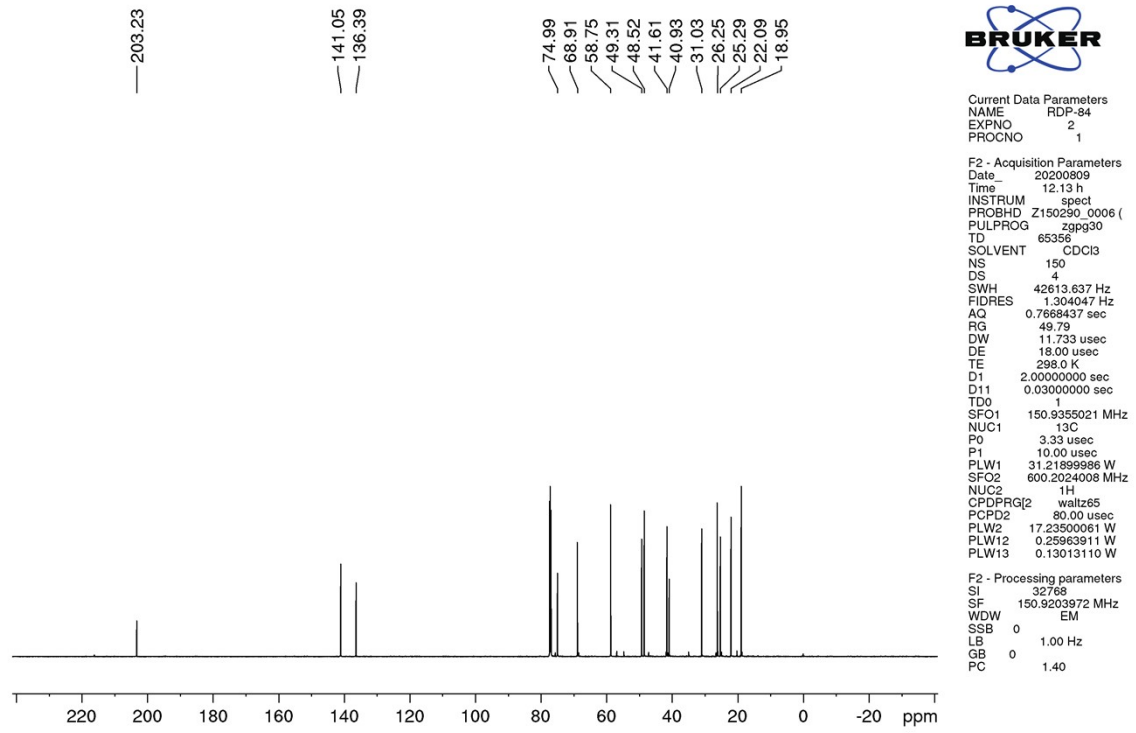

Figure S32 ^{13}C NMR spectrum (150 MHz, $CDCl_3$) of compound **4**

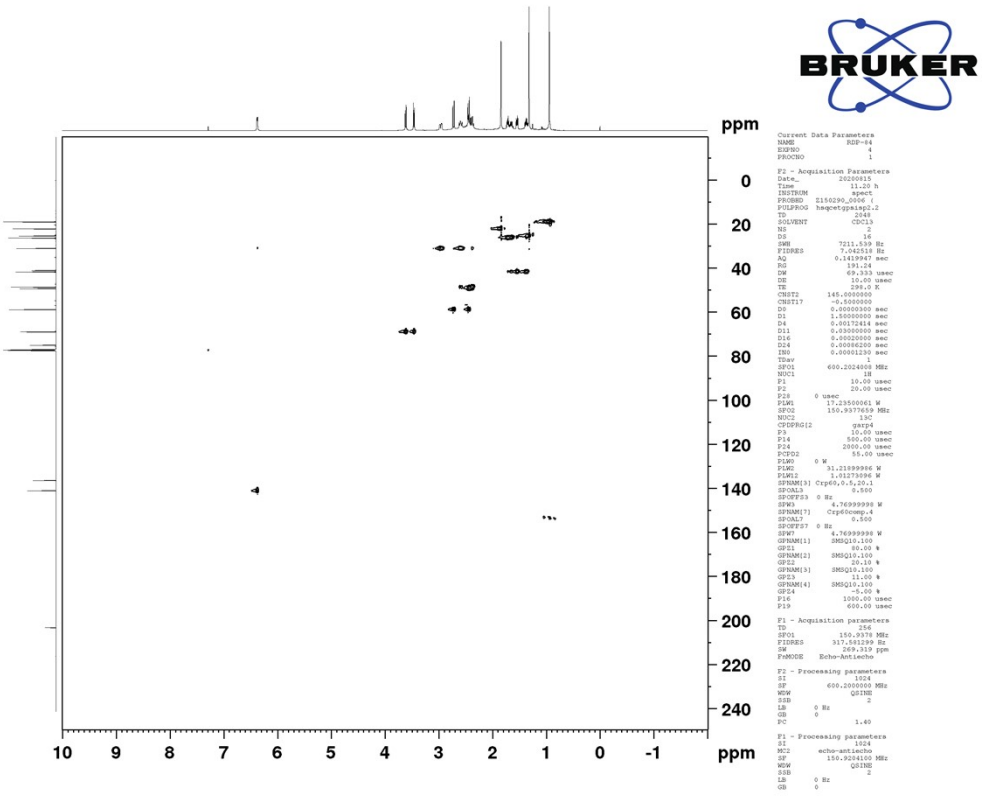

Figure S33 HSQC spectrum (600 MHz, $CDCl_3$) of compound **4**

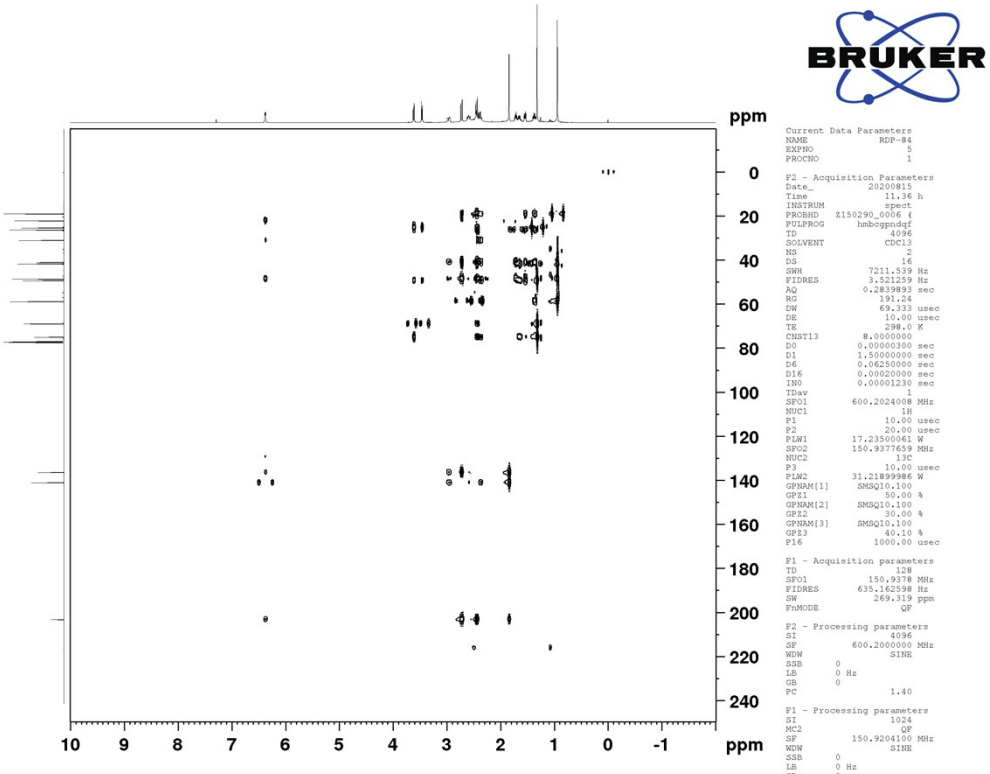

Figure S34 HMBC spectrum (600 MHz, $CDCl_3$) of compound **4**

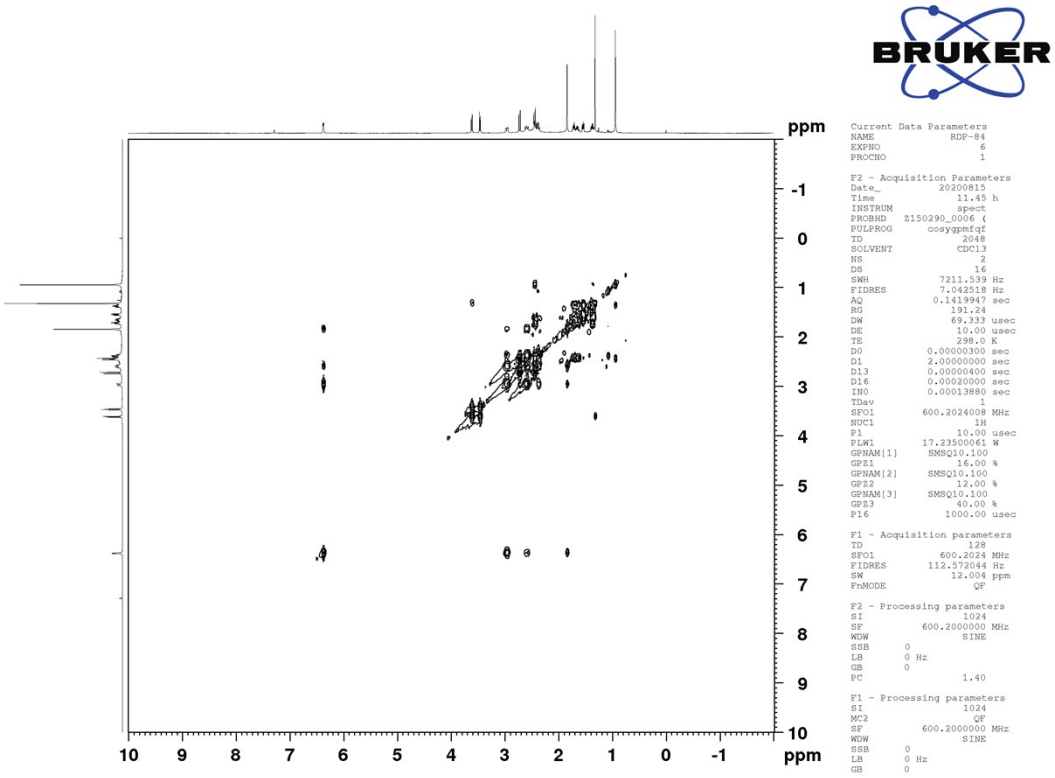

Figure S35 ^{1}H-^{1}H COSY spectrum (600 MHz, $CDCl_3$) of compound **4**

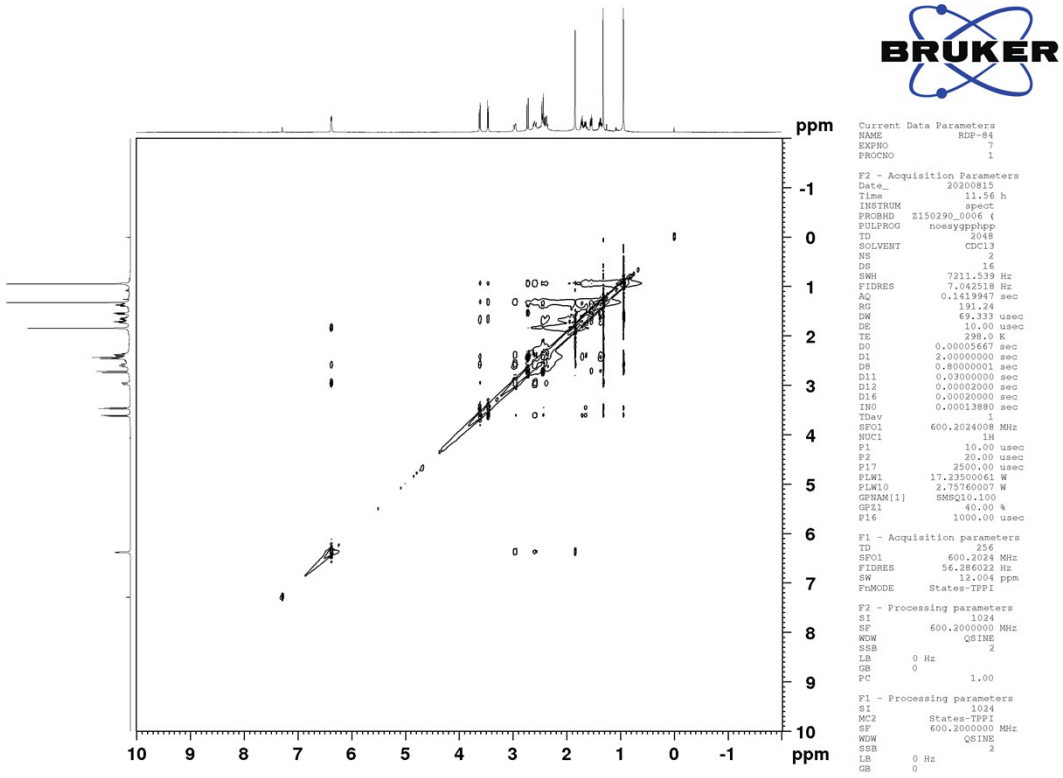

Figure S36 NOESY spectrum (600 MHz, $CDCl_3$) of compound **4**

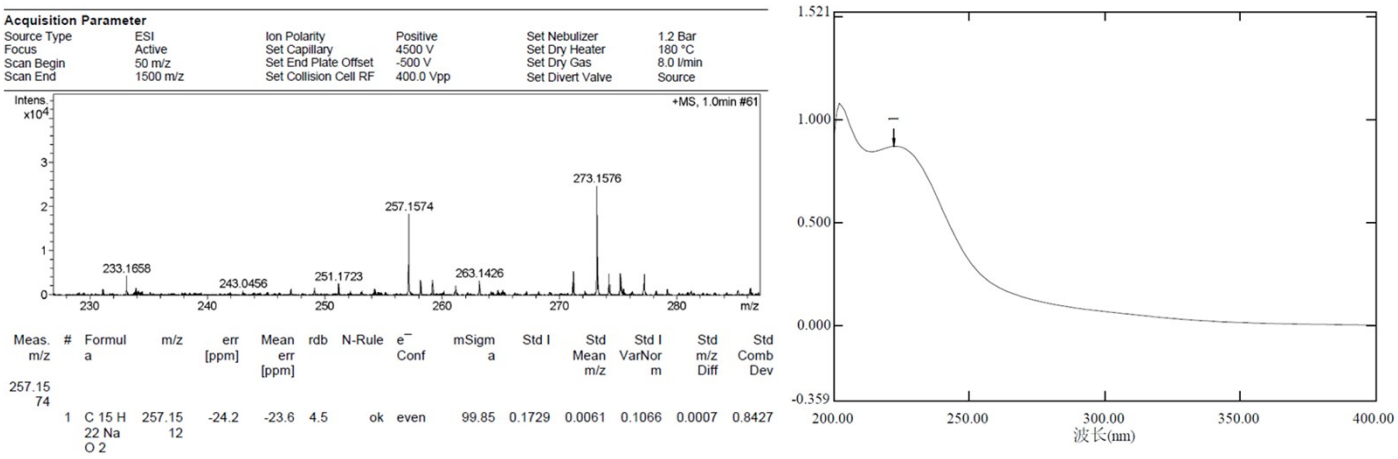

Figure S37 HRESIMS and UV spectra of compound **5**

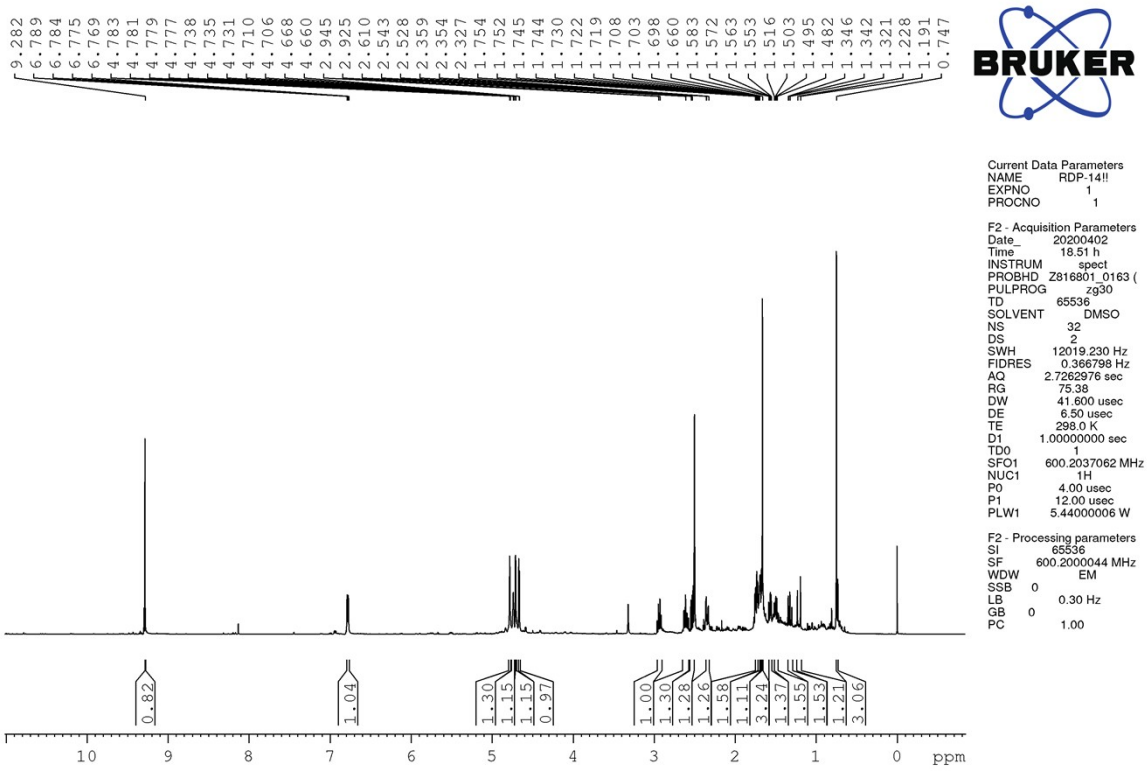

Figure S38 ^{1}H NMR spectrum (600 MHz, $CDCl_3$) of compound **5**

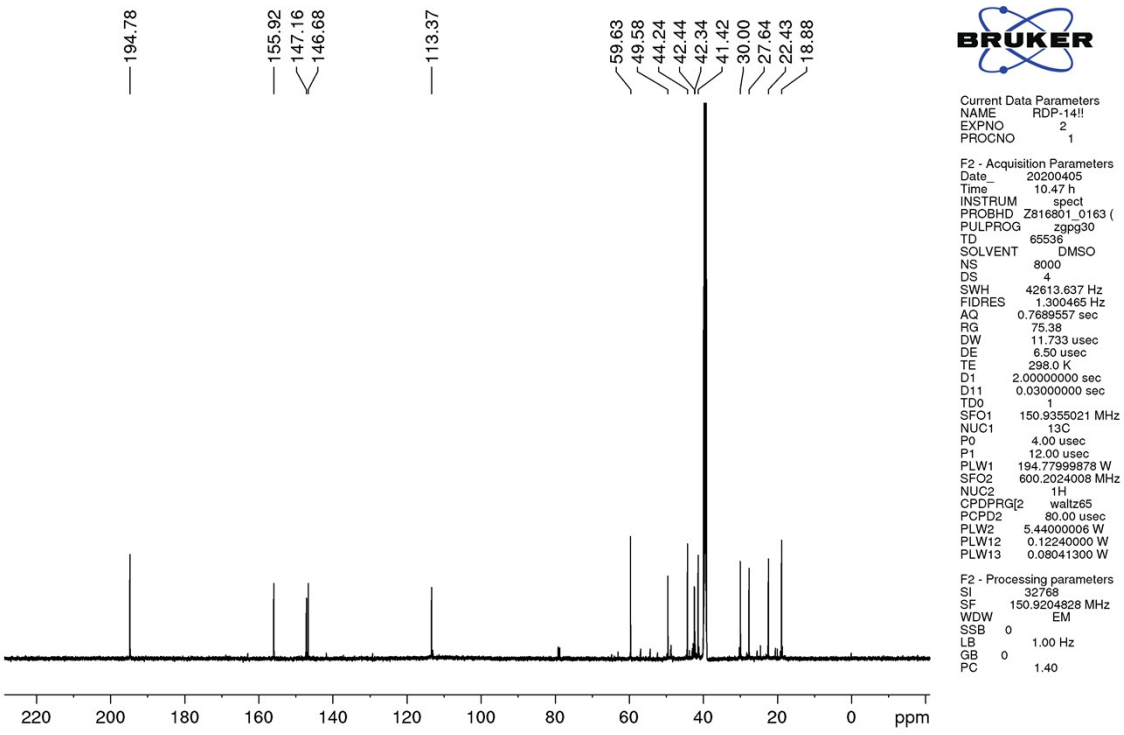

Figure S39 ^{13}C NMR spectrum (150 MHz, $CDCl_3$) of compound **5**

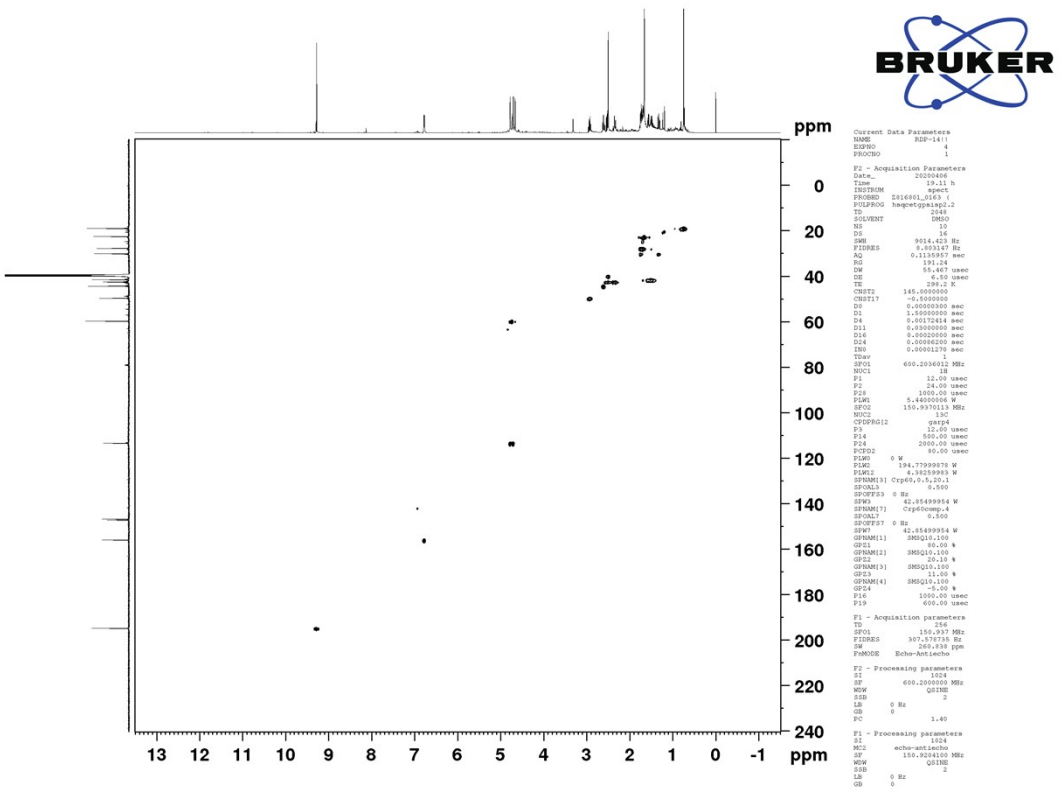

Figure S40 HSQC spectrum (600 MHz, $CDCl_3$) of compound **5**

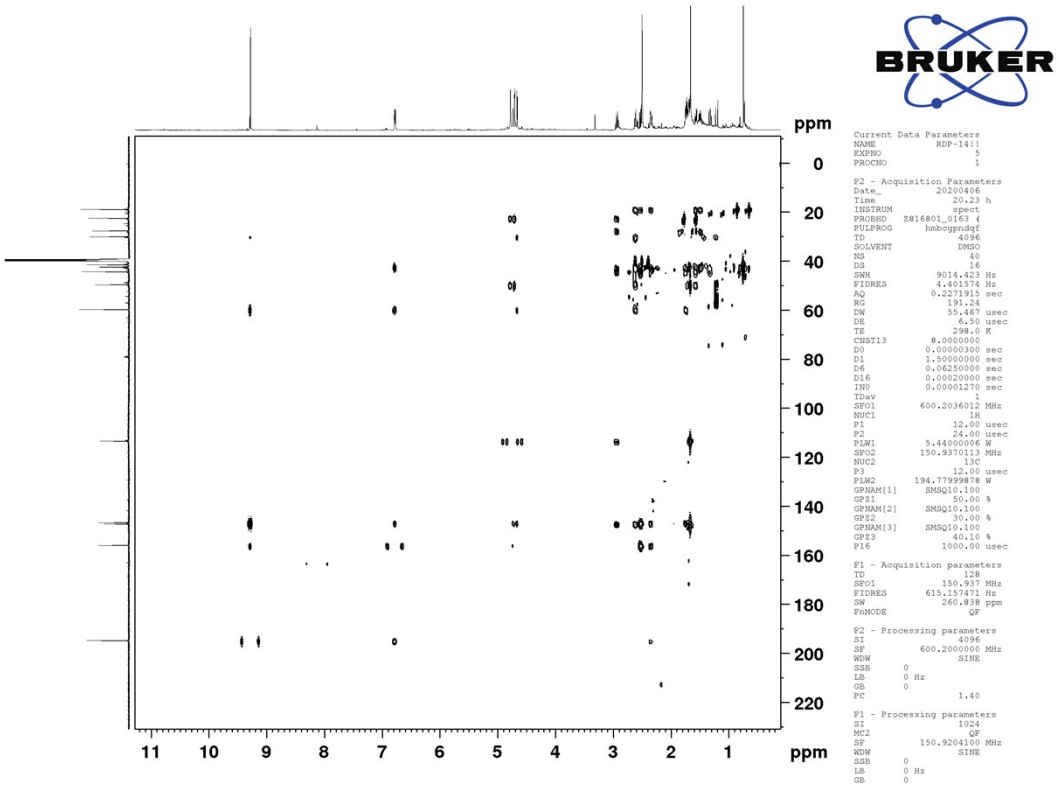

Figure S41 HMBC spectrum (600 MHz, $CDCl_3$) of compound **5**

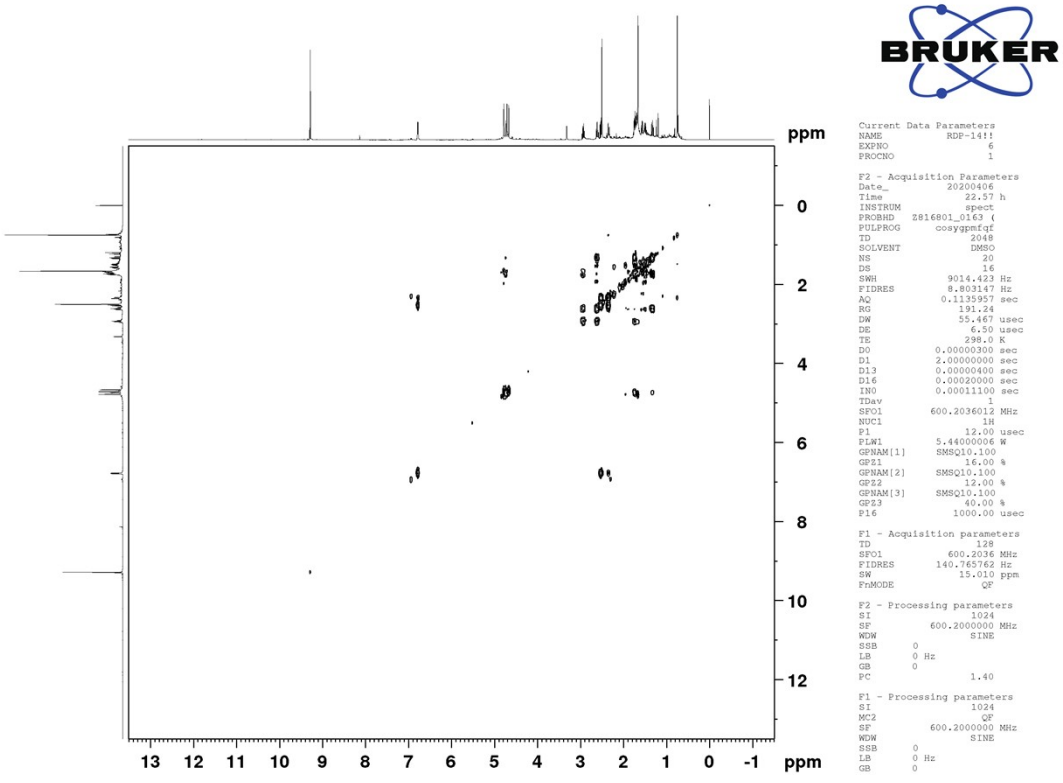

Figure S42 ^1H-^1H COSY spectrum (600 MHz, $CDCl_3$) of compound **5**

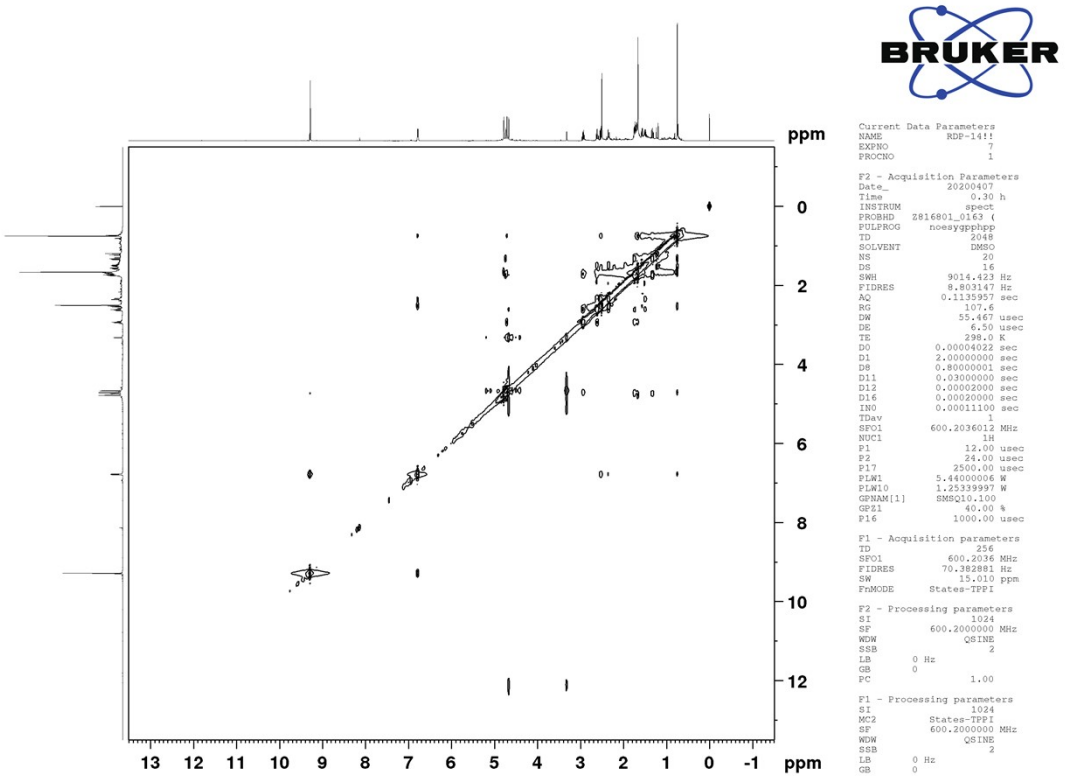

Figure S43 NOESY spectrum (600 MHz, $CDCl_3$) of compound **5**

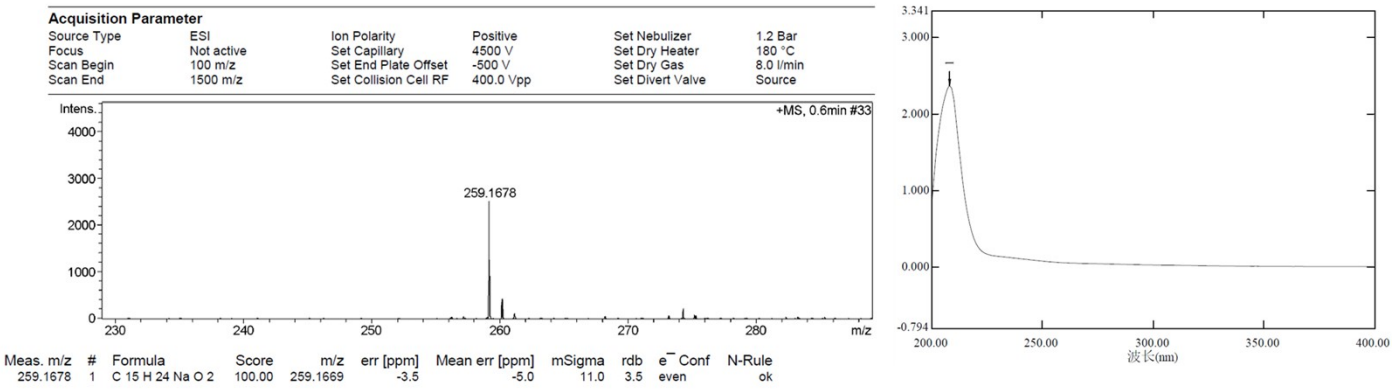

Figure S44 HRESIMS and UV spectra of compound **6**

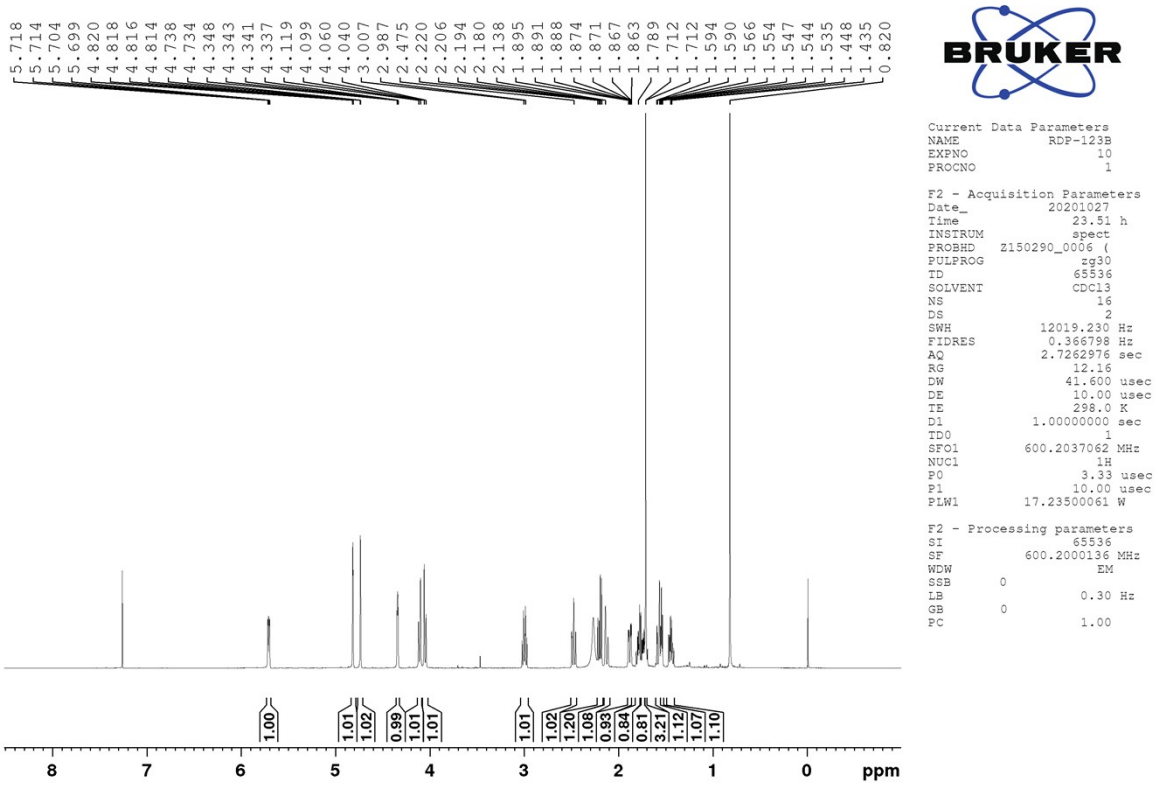

Figure S45 ^{1}H NMR spectrum (600 MHz, $CDCl_3$) of compound **6**

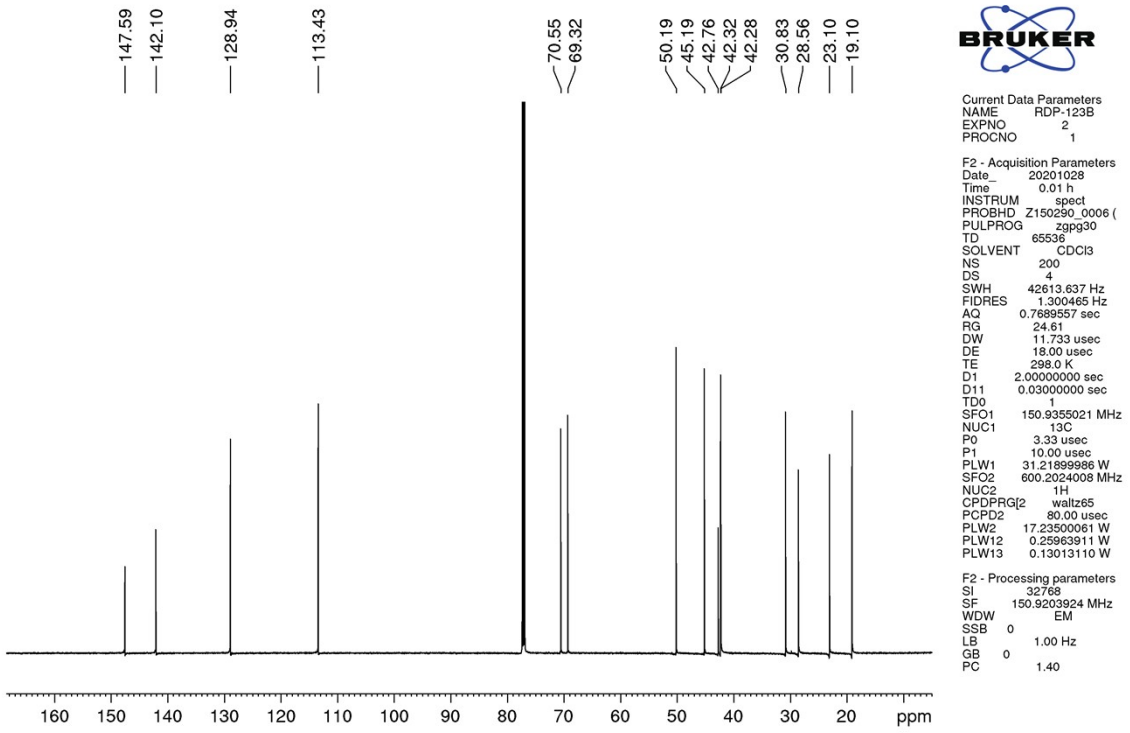

Figure S46 ^{13}C NMR spectrum (150 MHz, $CDCl_3$) of compound **6**

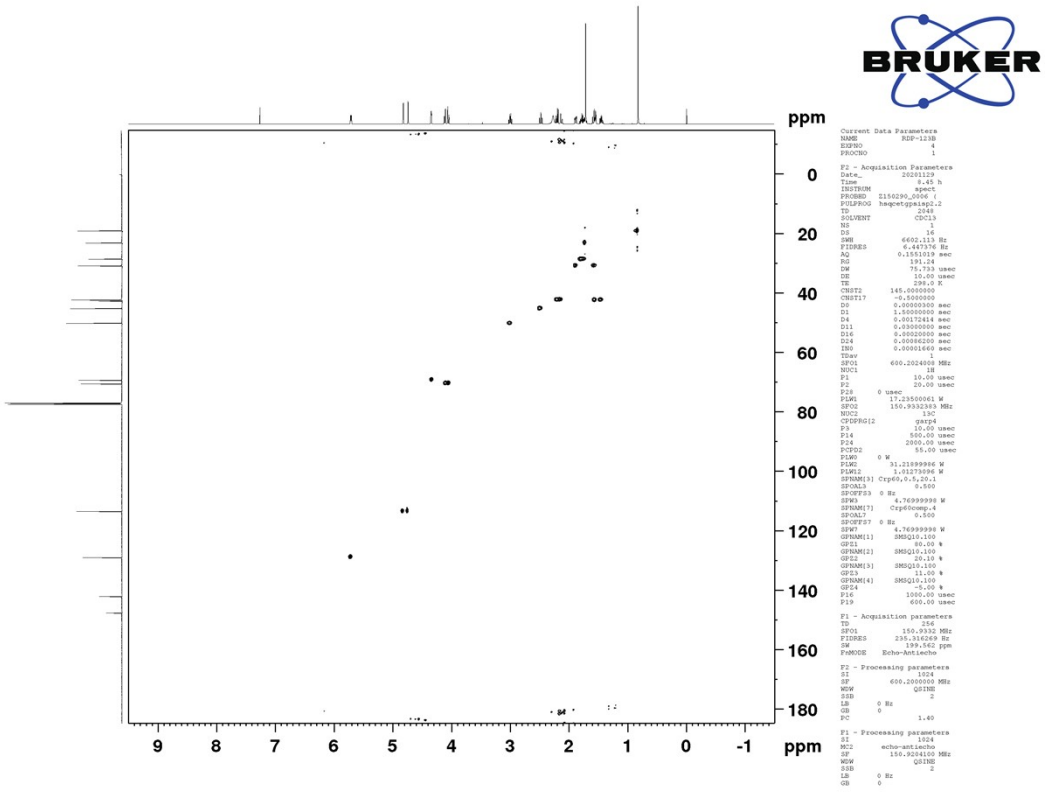

Figure S47 HSQC spectrum (600 MHz, $CDCl_3$) of compound **6**

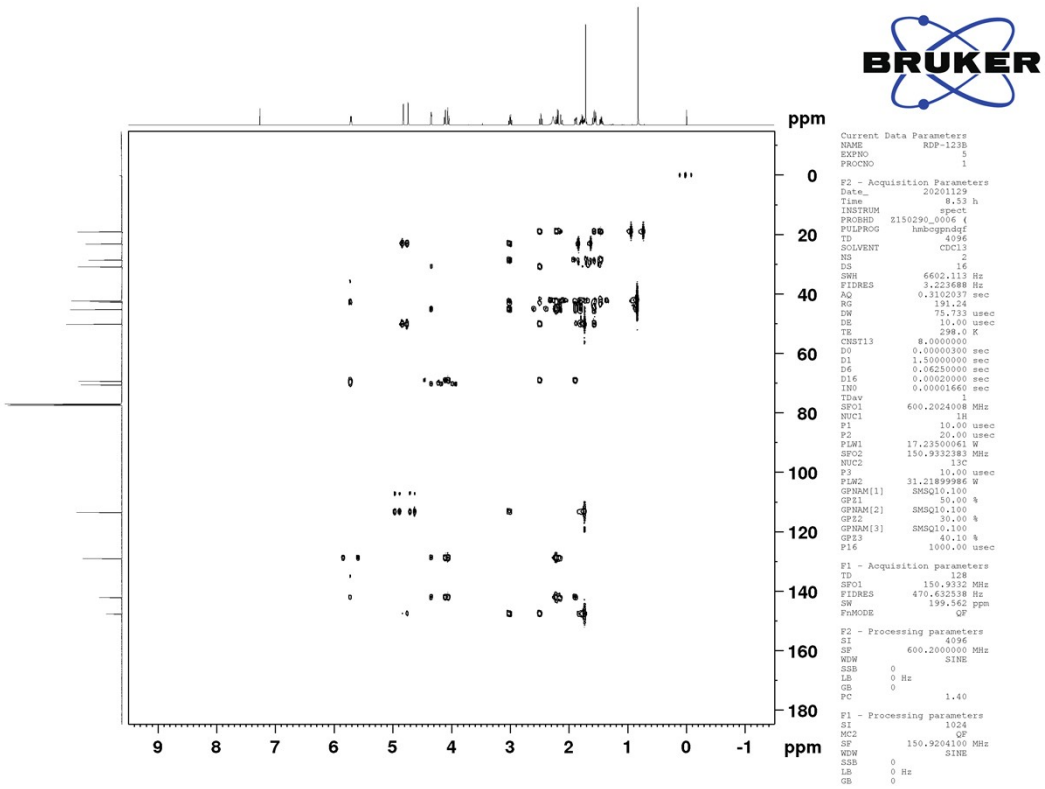

Figure S48 HMBC spectrum (600 MHz, $CDCl_3$) of compound **6**

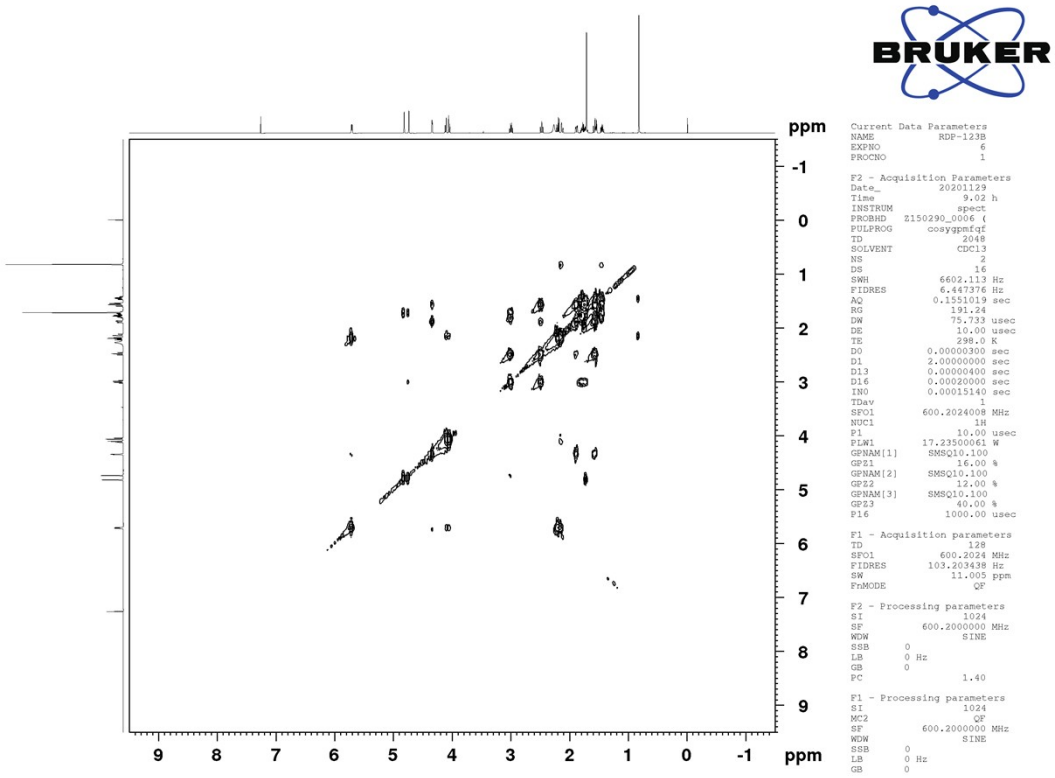

Figure S49 ^{1}H-^{1}H COSY spectrum (600 MHz, $CDCl_3$) of compound **6**

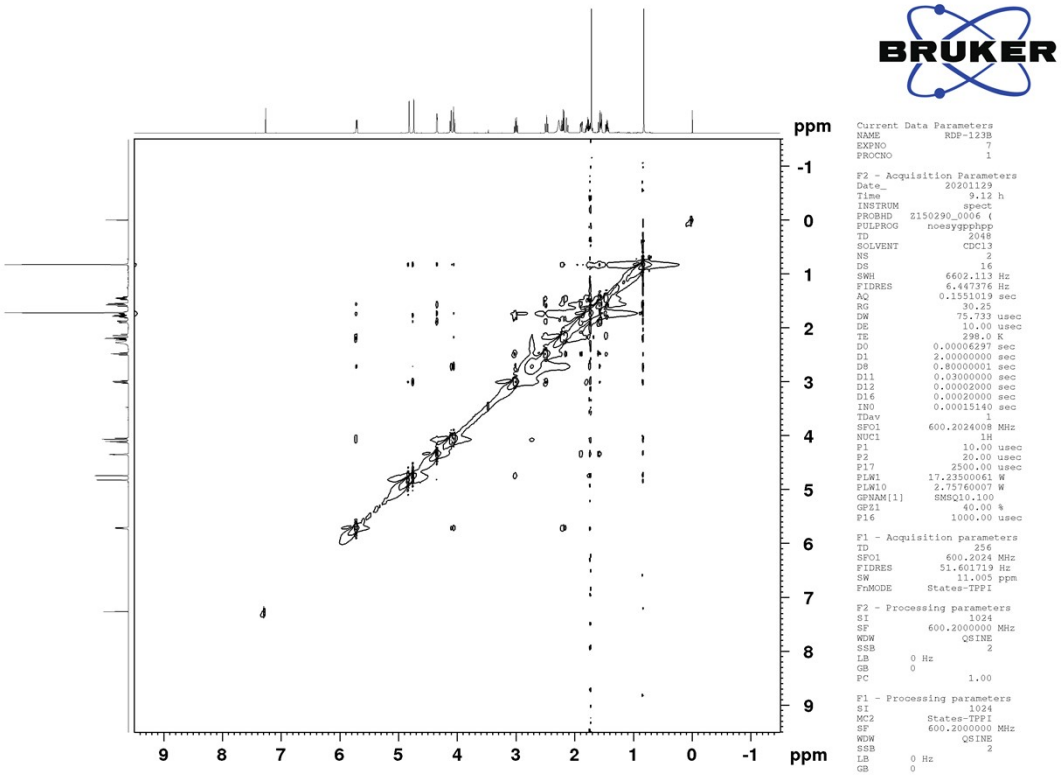

Figure S50 NOESY spectrum (600 MHz, $CDCl_3$) of compound **6**

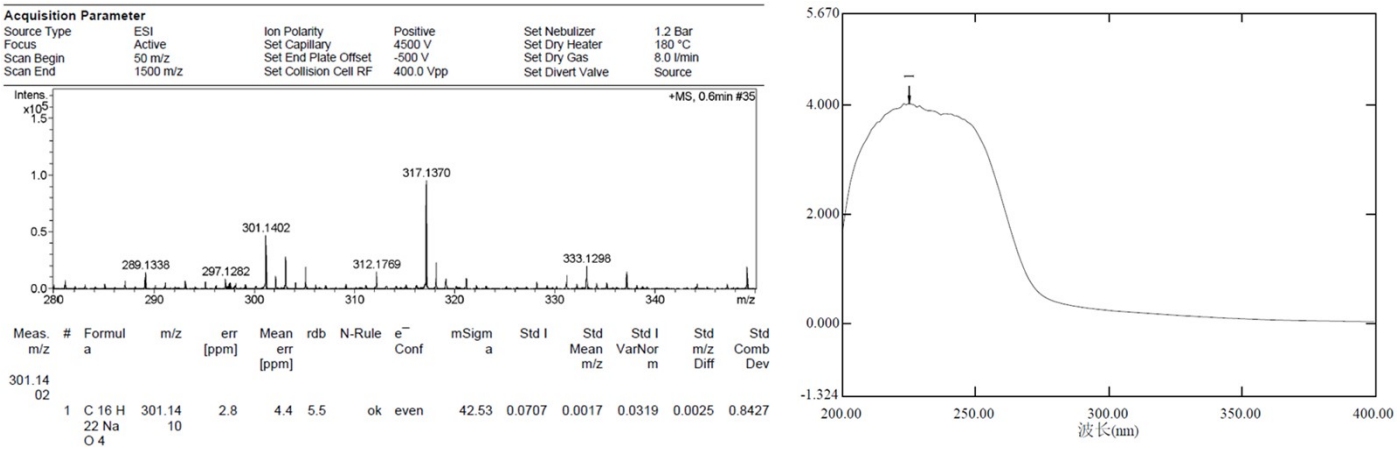

Figure S51 HRESIMS and UV spectra of compound **7**

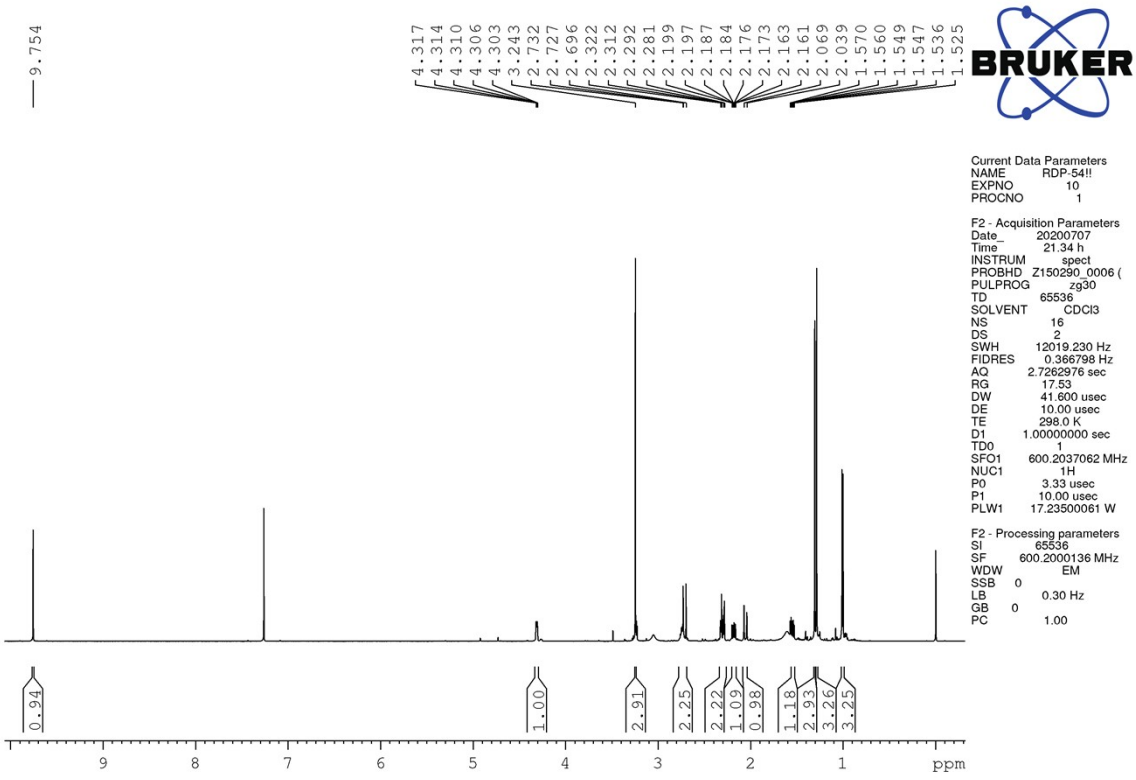

Figure S52 ^{1}H NMR spectrum (600 MHz, $CDCl_3$) of compound **7**

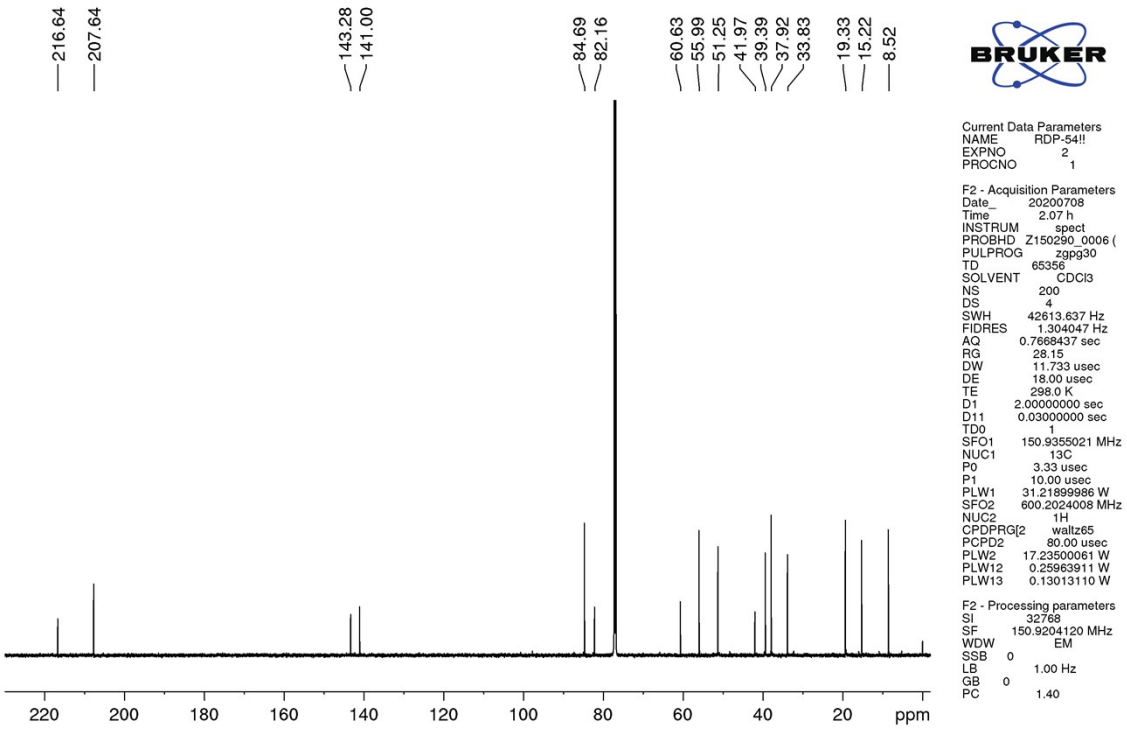

Figure S53 ^{13}C NMR spectrum (150 MHz, $CDCl_3$) of compound **7**

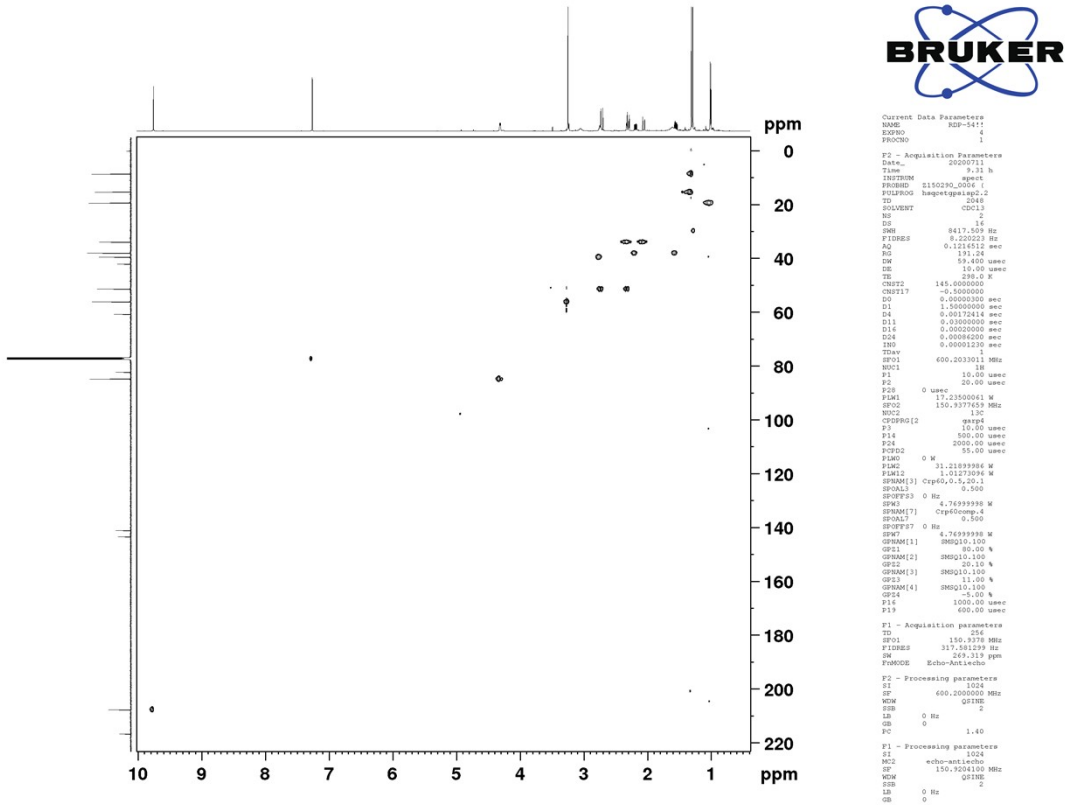

Figure S54 HSQC spectrum (600 MHz, $CDCl_3$) of compound **7**

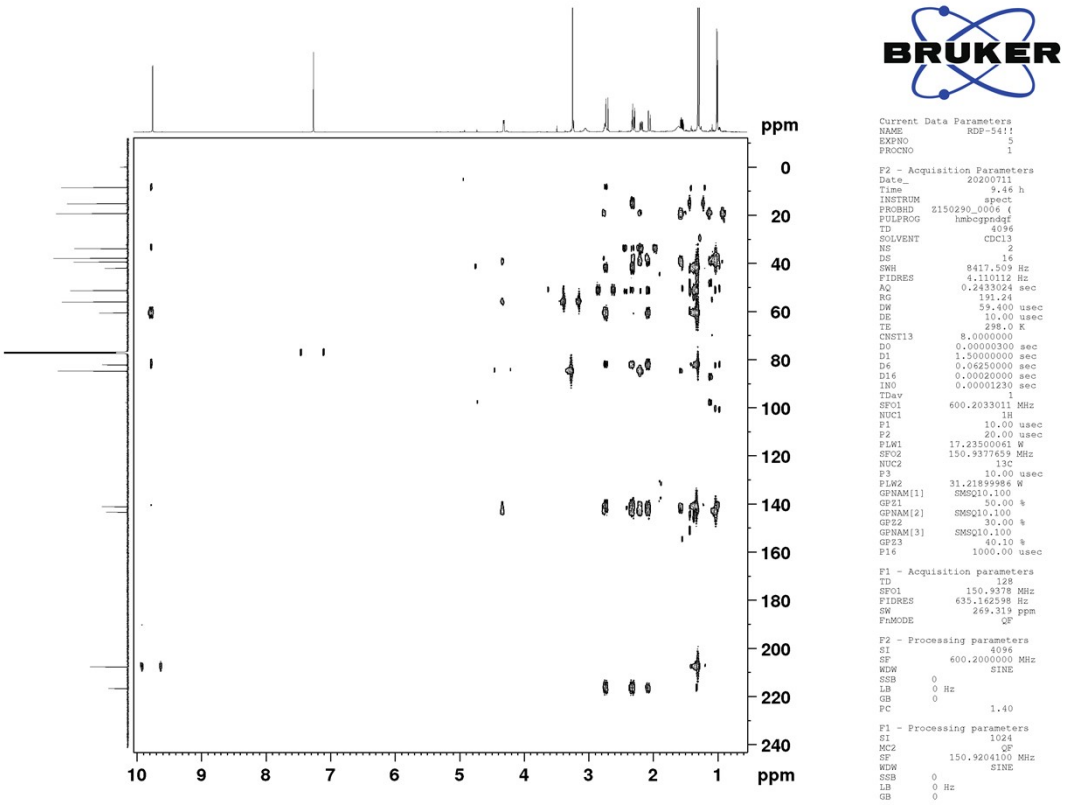

Figure S55 HMBC spectrum (600 MHz, $CDCl_3$) of compound **7**

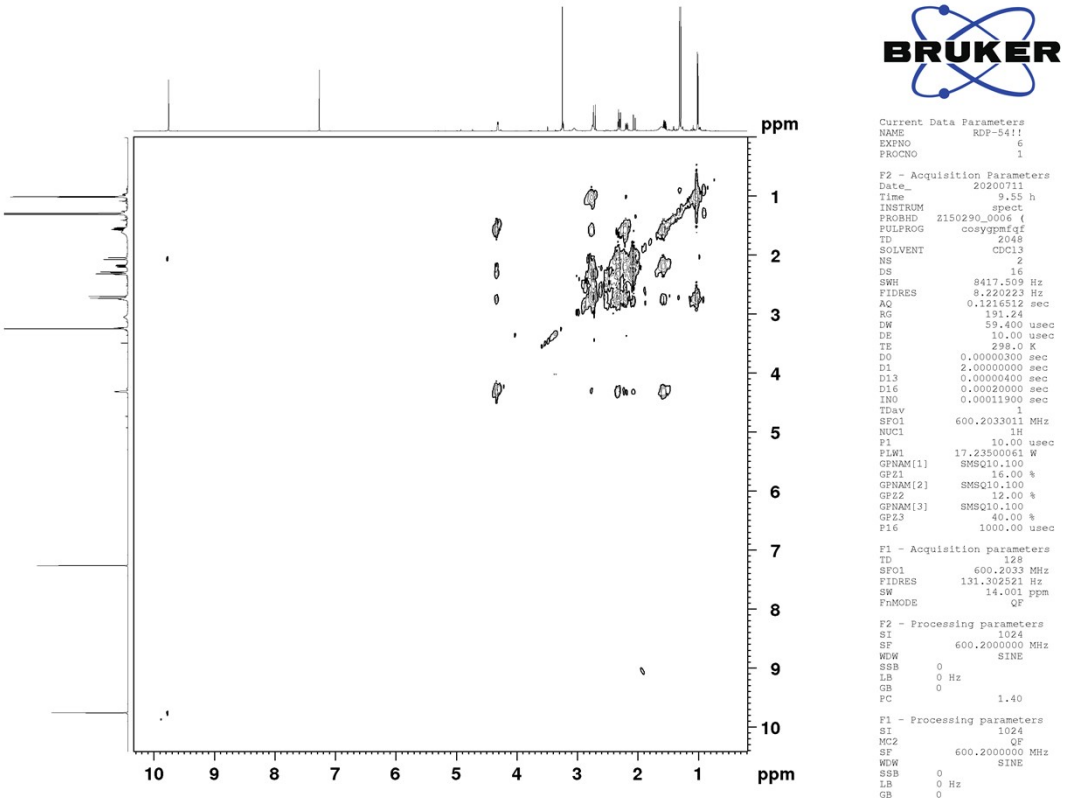

Figure S56 ^{1}H-^{1}H COSY spectrum (600 MHz, $CDCl_3$) of compound **7**

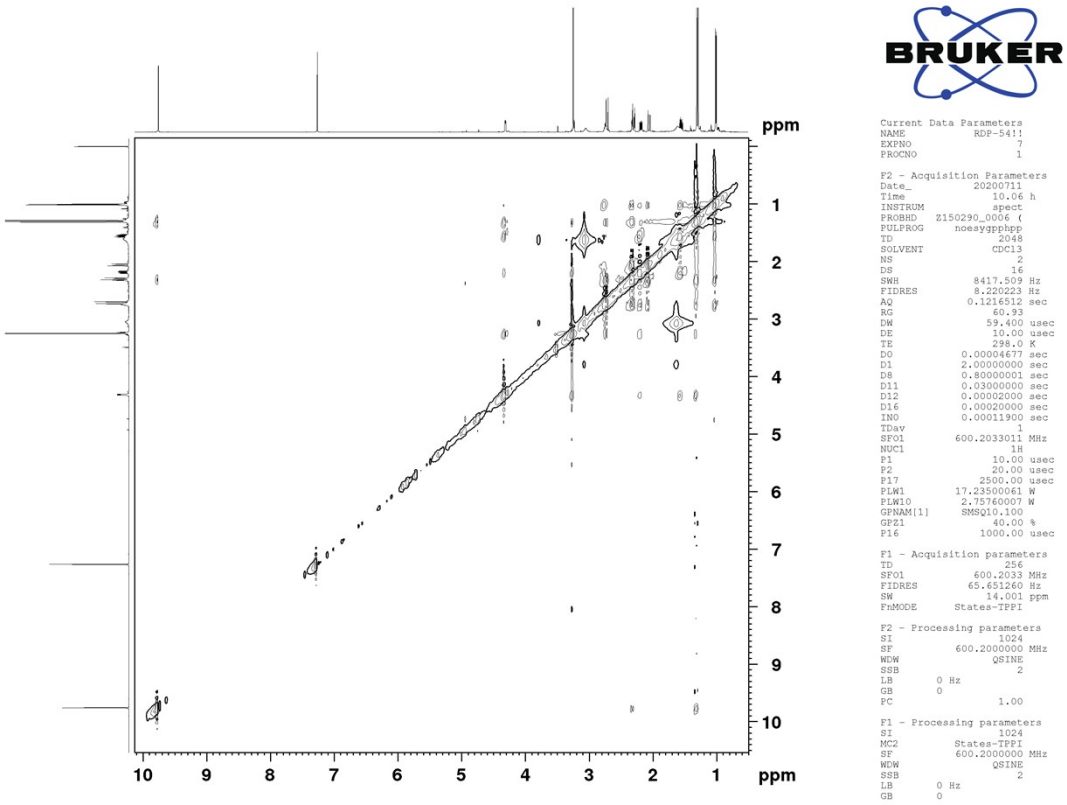

Figure S57 NOESY spectrum (600 MHz, $CDCl_3$) of compound **7**

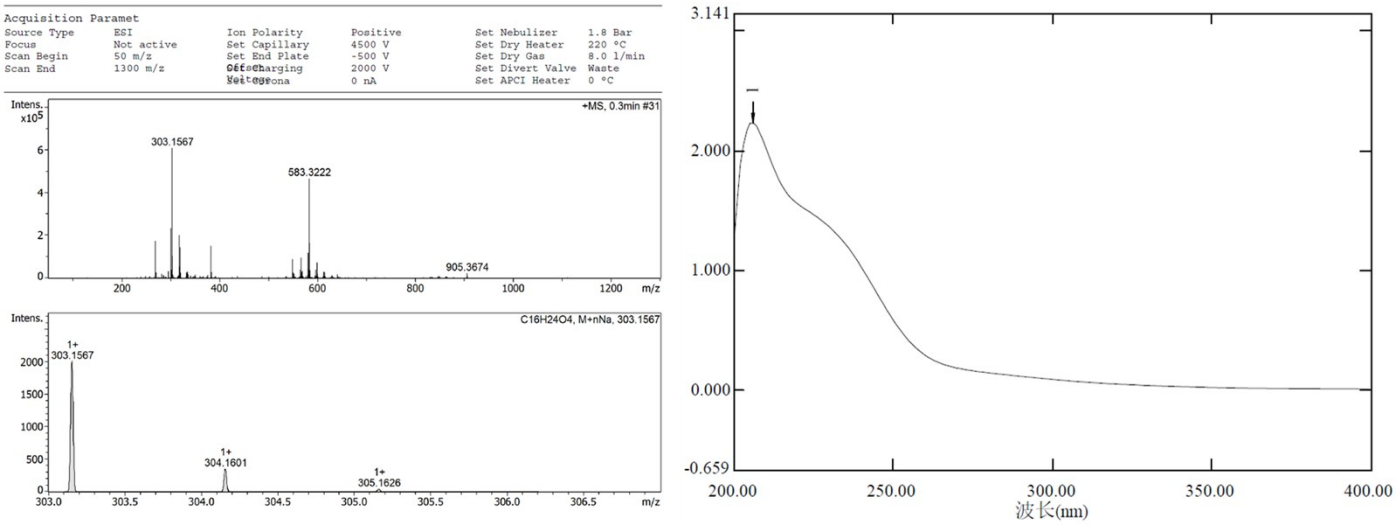

Figure S58 HRESIMS and UV spectra of compound **8**

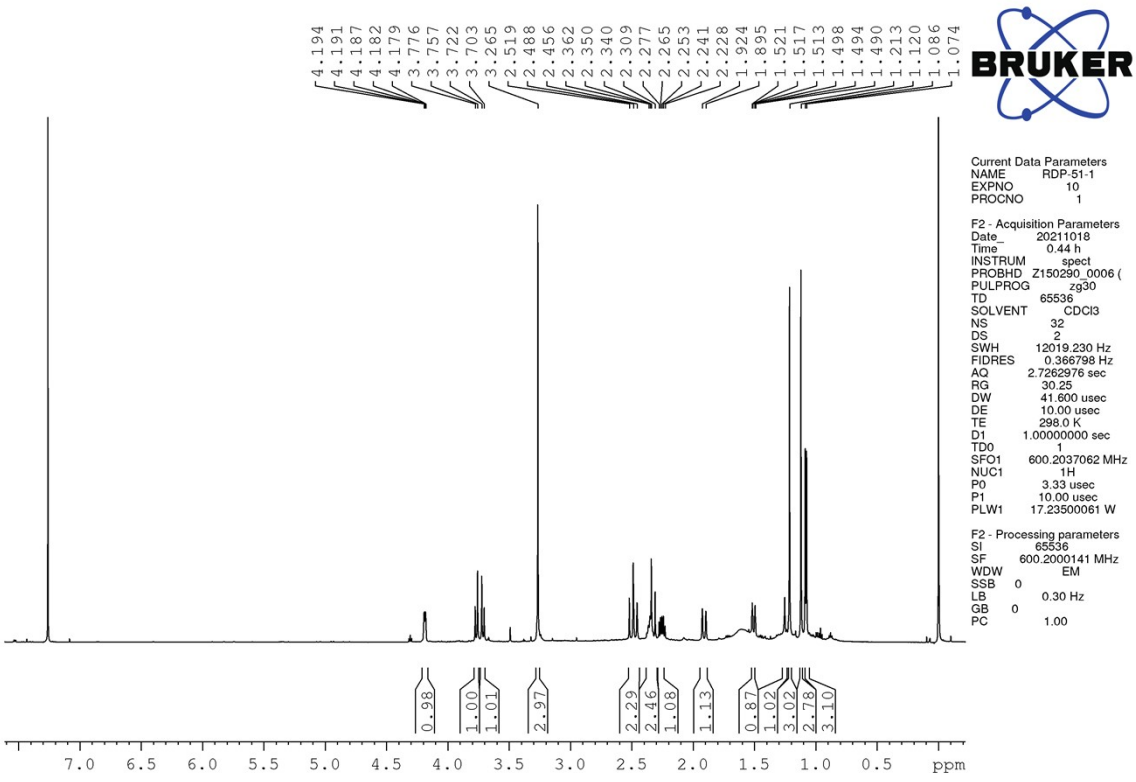

Figure S59 ^{1}H NMR spectrum (600 MHz, $CDCl_3$) of compound **8**

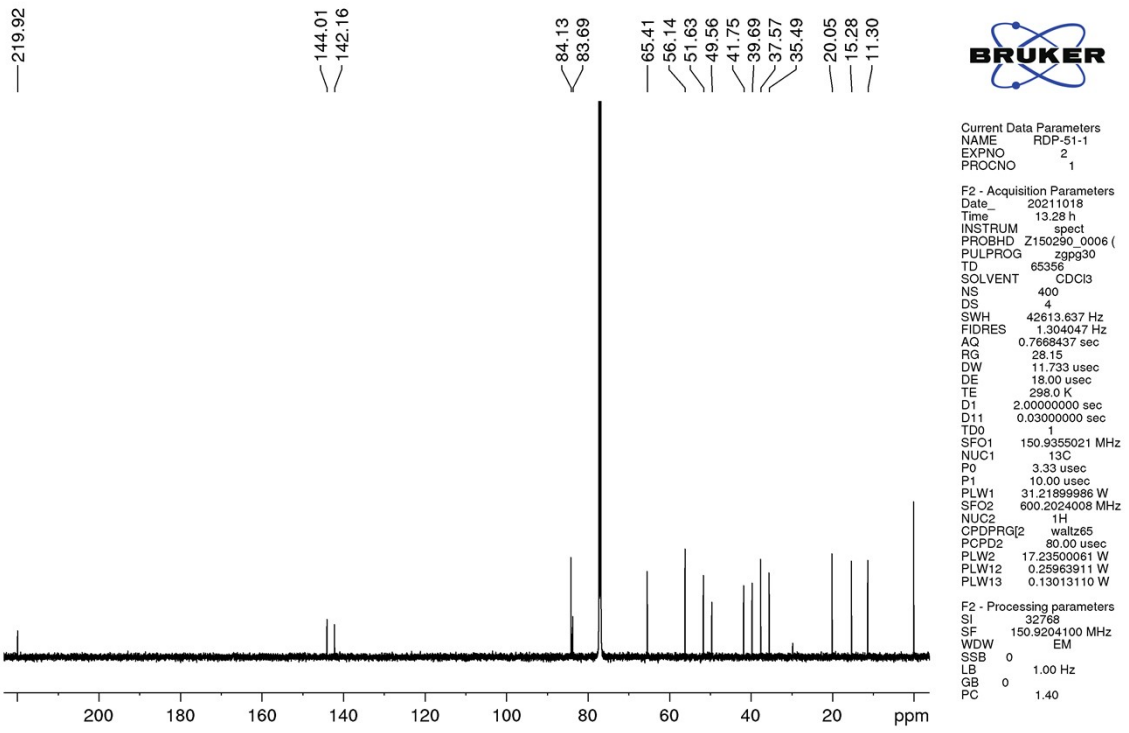

Figure S60 ^{13}C NMR spectrum (150 MHz, $CDCl_3$) of compound **8**

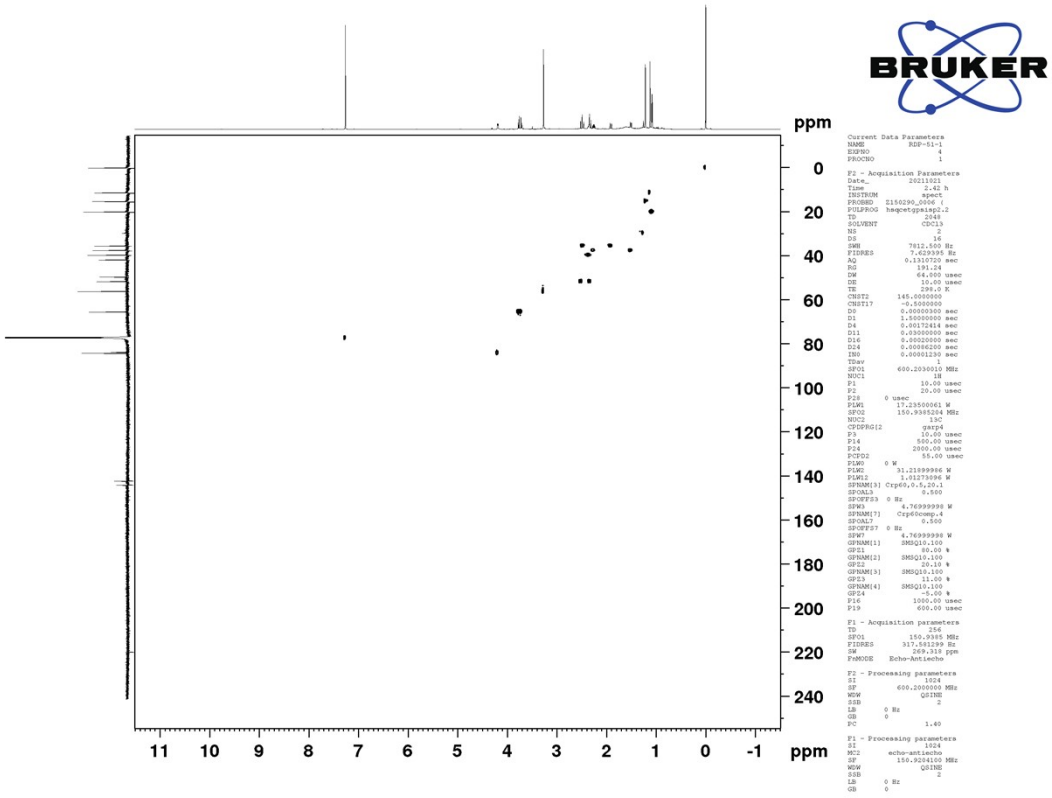

Figure S61 HSQC spectrum (600 MHz, $CDCl_3$) of compound **8**

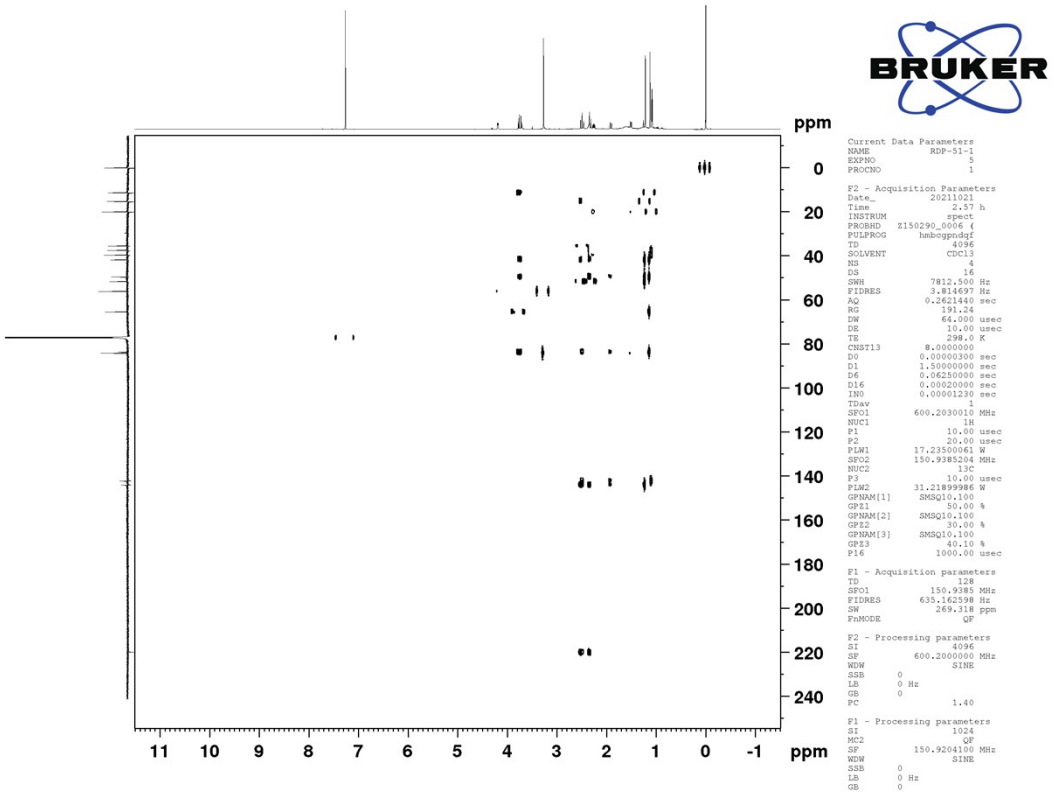

Figure S62 HMBC spectrum (600 MHz, $CDCl_3$) of compound **8**

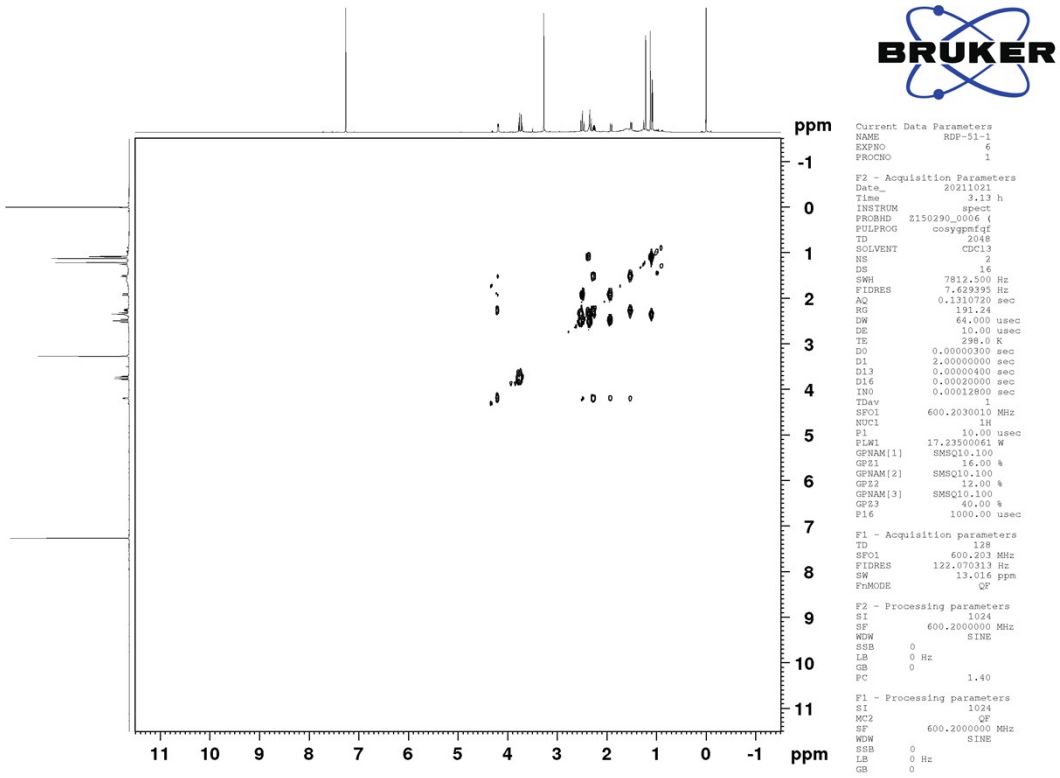

Figure S63 ^{1}H-^{1}H COSY spectrum (600 MHz, $CDCl_3$) of compound **8**

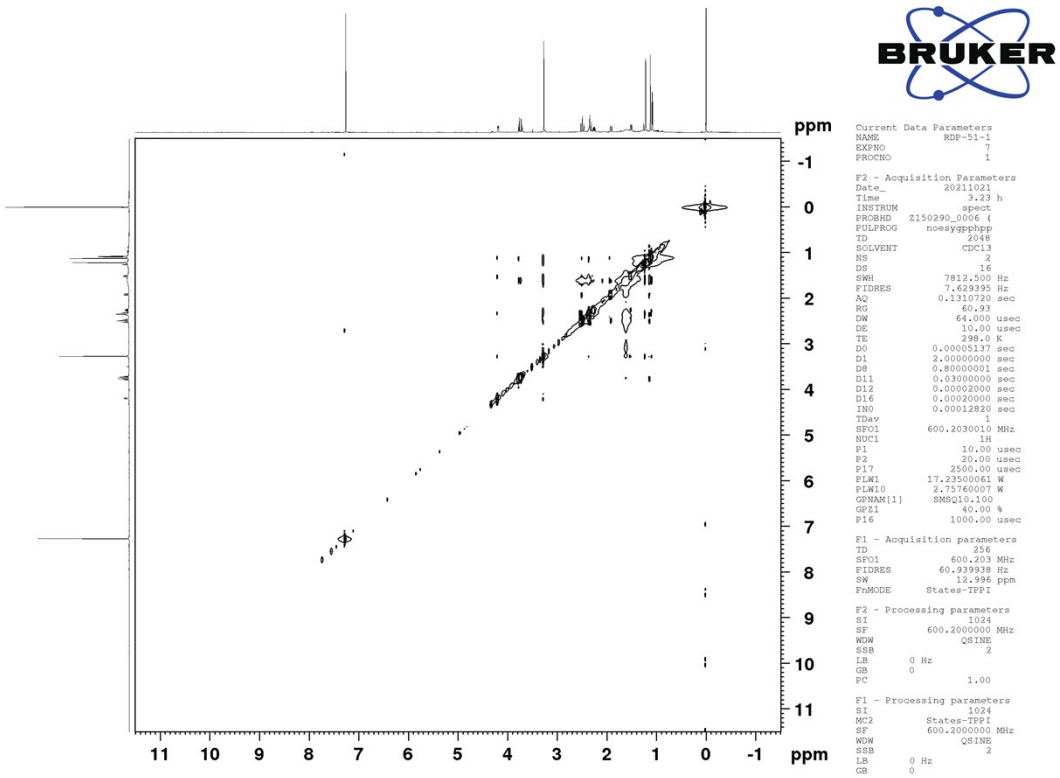

Figure S64 NOESY spectrum (600 MHz, $CDCl_3$) of compound **8**

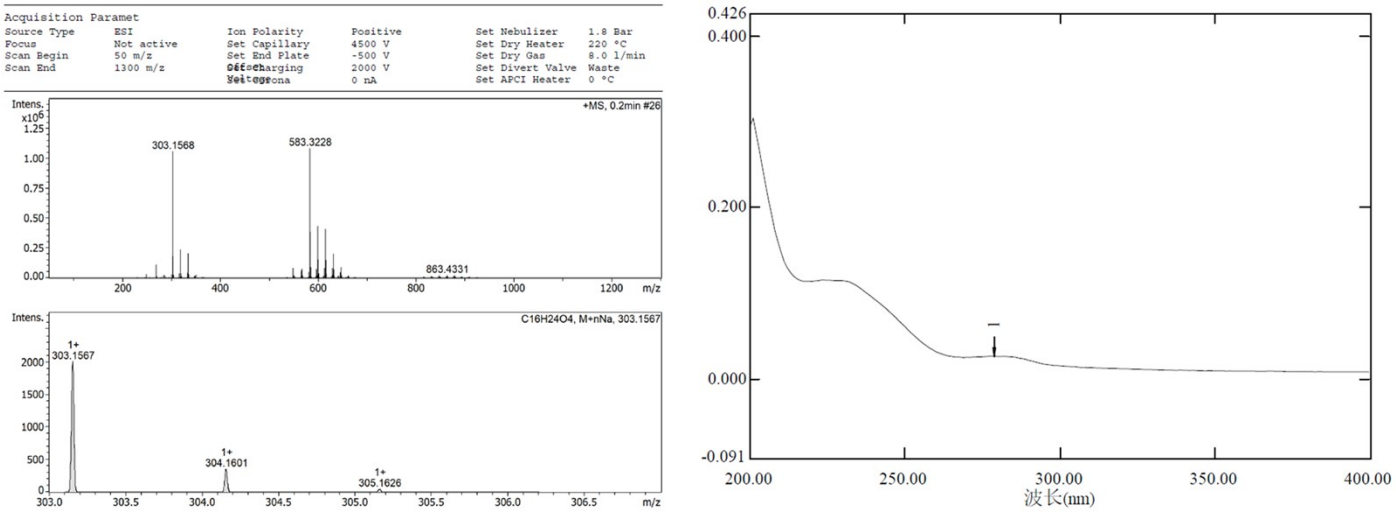

Figure S65 HRESIMS and UV spectra of compound **9**

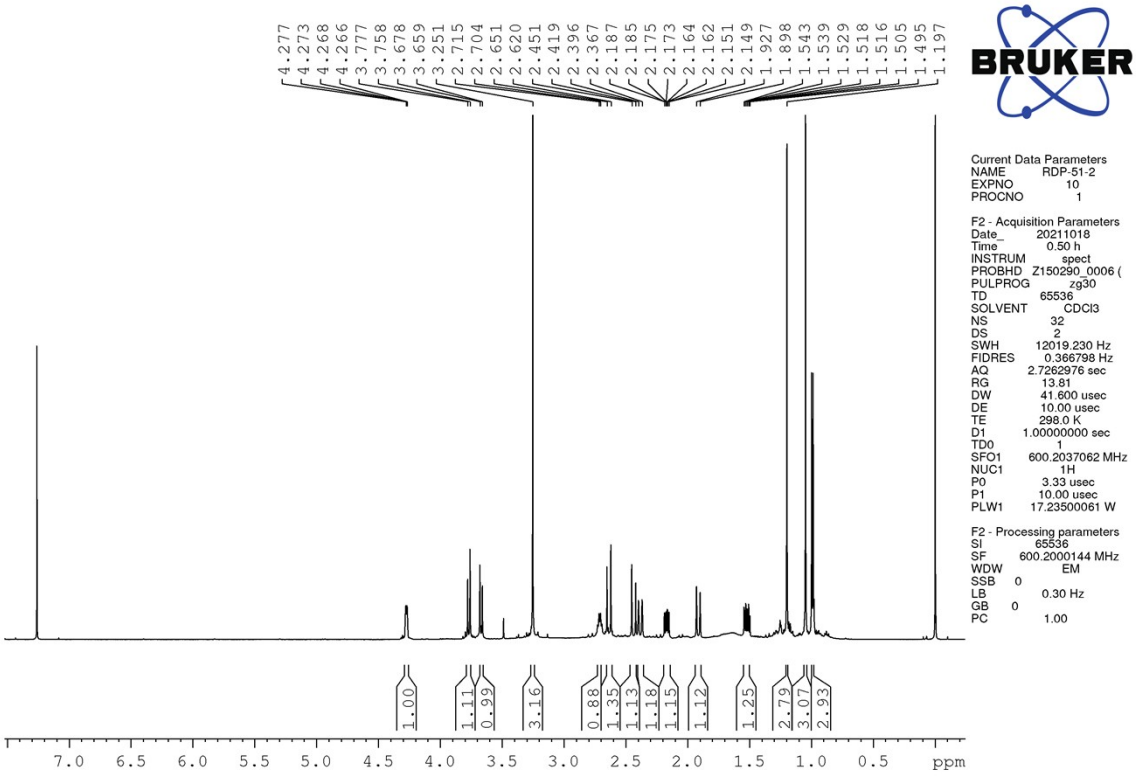

Figure S66 ^{1}H NMR spectrum (600 MHz, $CDCl_3$) of compound **9**

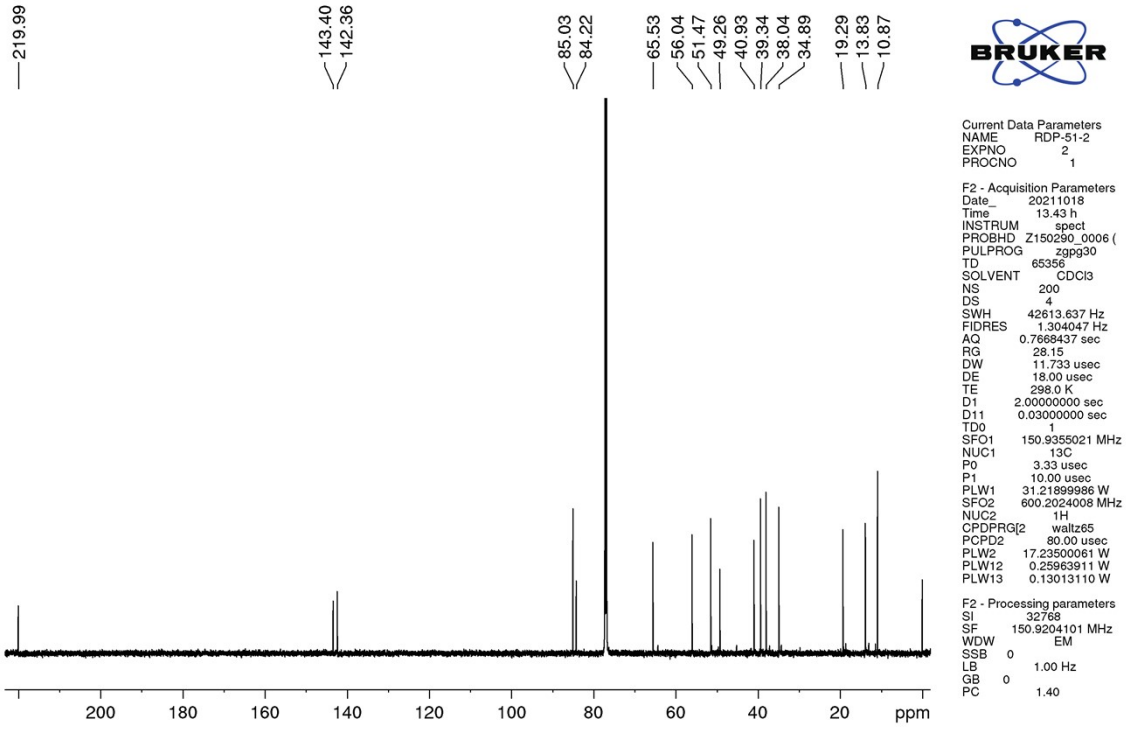

Figure S67 ^{13}C NMR spectrum (150 MHz, $CDCl_3$) of compound **9**

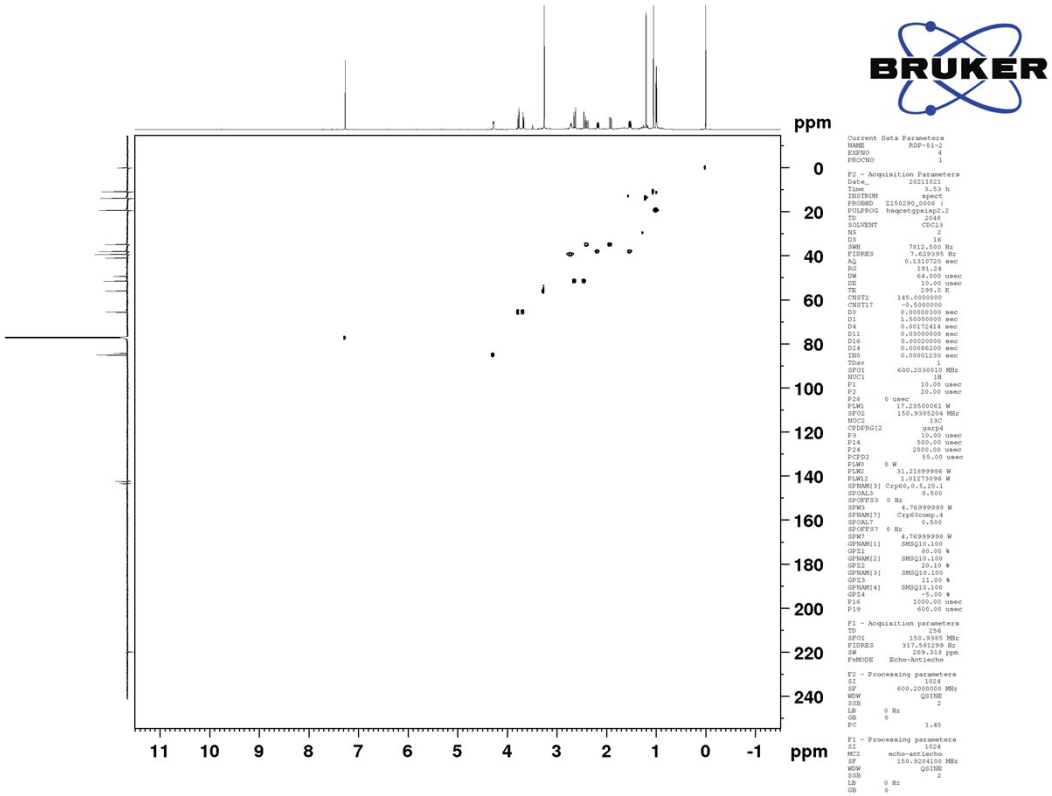

Figure S68 HSQC spectrum (600 MHz, $CDCl_3$) of compound **9**

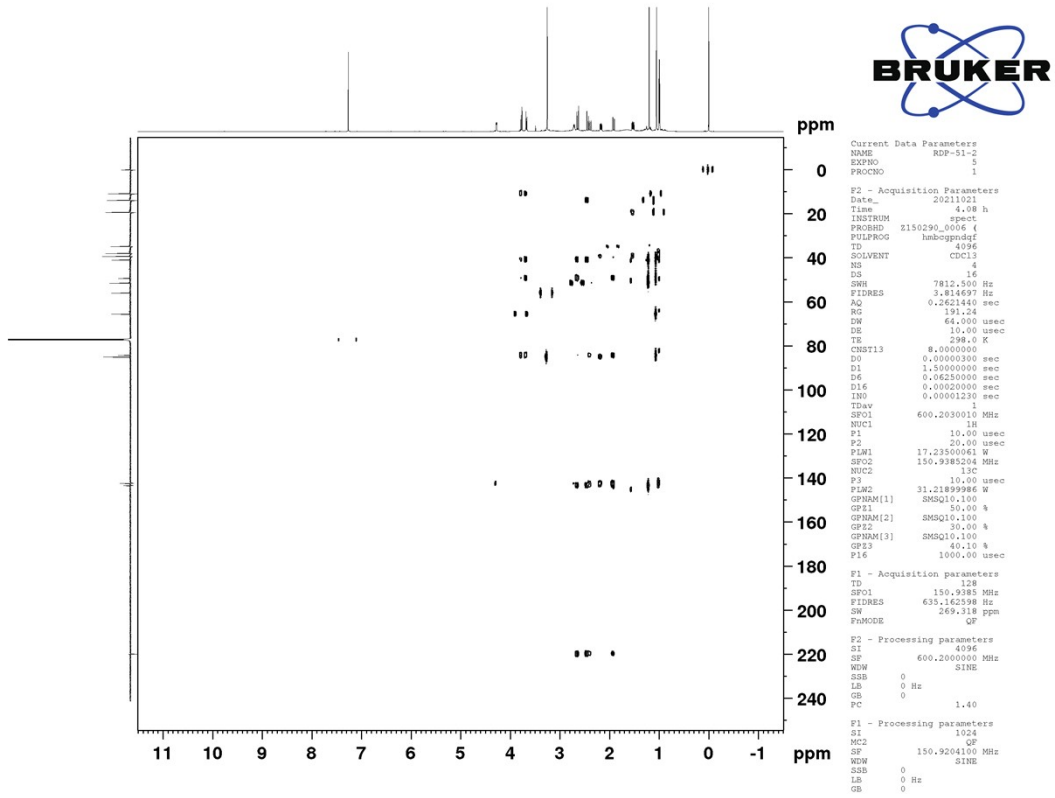

Figure S69 HMBC spectrum (600 MHz, $CDCl_3$) of compound **9**

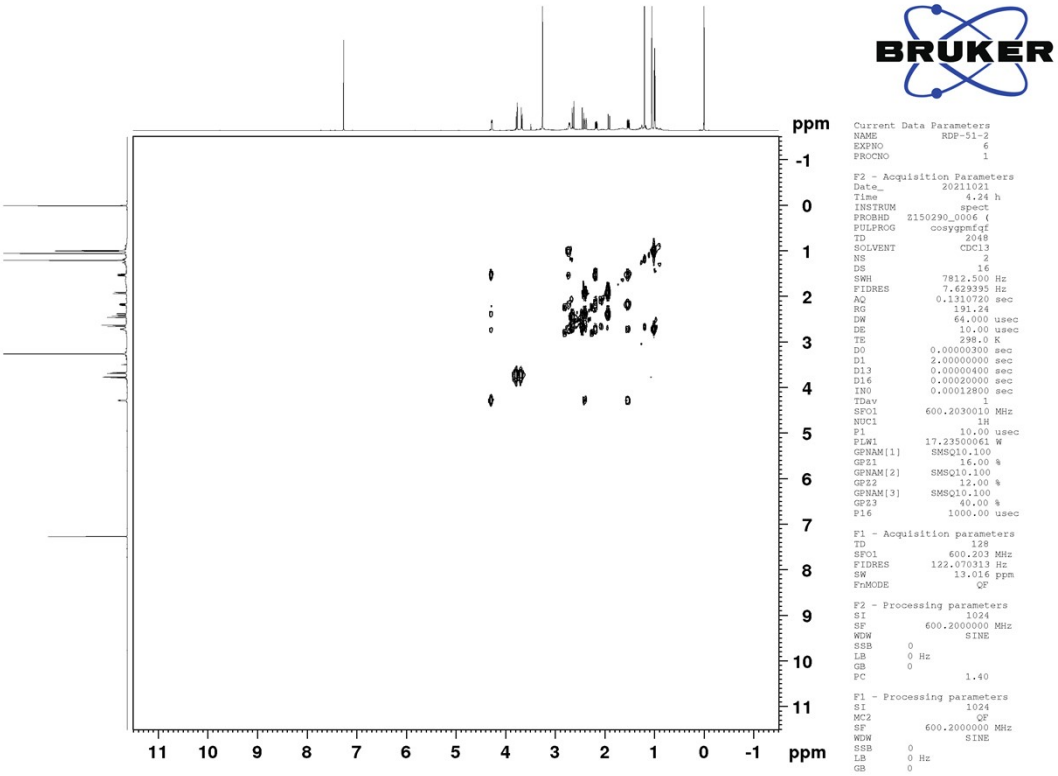

Figure S70 ^1H-^1H COSY spectrum (600 MHz, $CDCl_3$) of compound **9**

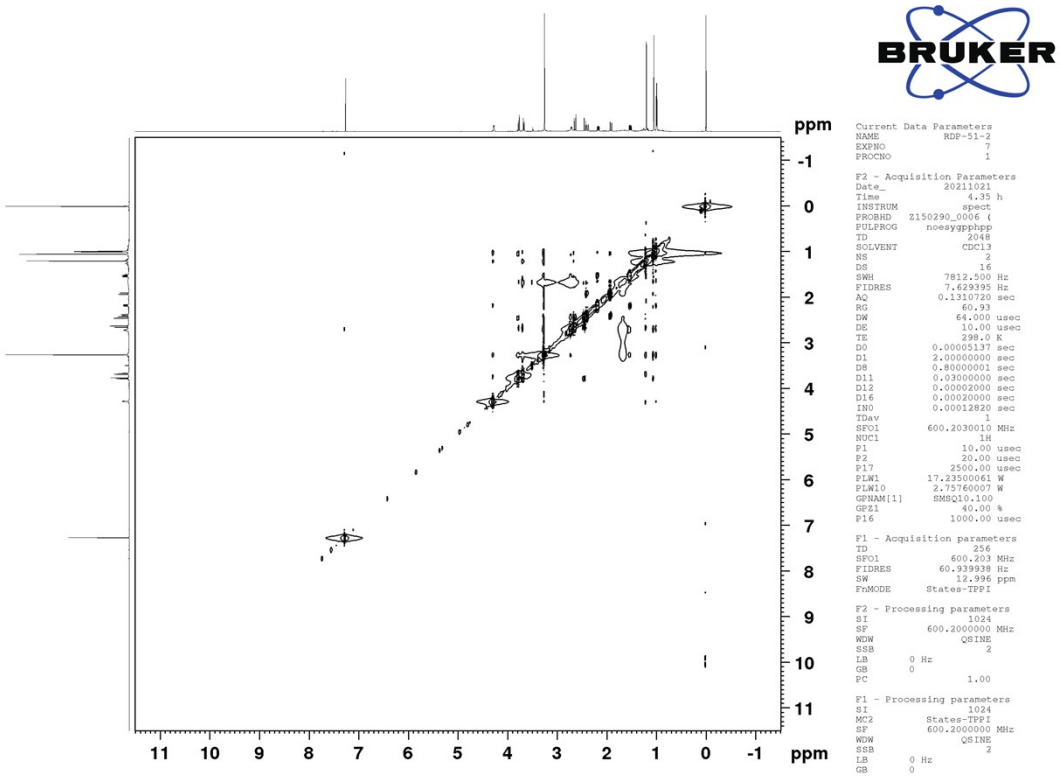

Figure S71 NOESY spectrum (600 MHz, $CDCl_3$) of compound **9**

Table S1 Cytotoxicities of compounds **1**–**11** against Hep3B and HepG2 cells (IC_{50}, μM)

compound	Hep3B	HepG2	compound	Hep3B	HepG2
1	>50	>50	**7**	37.45 ± 0.42	>50
2	21.66 ± 1.82	>50	**8**	17.11 ± 0.78	>50
3	33.90 ± 0.92	>50	**9**	17.95 ± 1.12	>50
4	22.11 ± 1.98	>50	**10**	>50	>50
5	37.53 ± 0.88	>50	**11**	33.42 ± 1.38	>50
6	36.36 ± 0.29	>50	sorafenib[a]	5.48± 0.25	11.67 ± 0.58

Data presented as Mean ± SD (n = 3).

[a] Positive control